2008

STRANDED CORE TRANSFORMER LOSS ANALYSIS

Xingxing Zhang
University of Kentucky, xingzhang@uky.edu

ABSTRACT OF THESIS

STRANDED CORE TRANSFORMER LOSS ANALYSIS

We will present the approaches used to investigating the power loss for the stranded core transformers. One advantage of using stranded core is to reduce power loss or enhance transformer efficiency. One difficulty in the modeling of this type of transformer is that the core is not solid (there are small gaps between core wires due to circular cross section). A two dimensional finite element method with nodal basis function for magnetostatic field was developed to study the effects of the small gaps between core wires. The magnetic flux densities are compared for the uniform (solid) cores and the stranded cores for various permeability values. The effects of different air gap dimensions in stranded core to the magnitude of magnetic flux density were also discussed. The results of the two dimensional study were applied to modify the B-H curves in a 3D simulation with an equivalent simplified uniformed core transformer model via Ansoft Maxwell 3D. This is achieved by output the magnitude of magnetic flux density at fixed points of mesh center. The total core loss of a transformer was predicted by integration of the losses of all elements.

KEYWORDS: Stranded Core Transformer, FEM, B-H Curve, Iron Loss, Air Gap

Xingxing Zhang

Apr. 10th. 2008

STRANDED CORE TRANSFORMER LOSS ANALYSIS

By

Xingxing Zhang

Cai-Cheng Lu
Director of Thesis

Yu Ming Zhang
Director of Graduate Studies

Apr. 10th. 2008

RULES FOR THE USE OF THESES

Unpublished theses submitted for the Master's degree and deposited in the University of Kentucky Library are as a rule open for inspection, but are to be used only with due regard to the rights of the authors. Bibliographical references may be noted, but quotations or summaries of parts may be published only with the permission of the author, and with the usual scholarly acknowledgments.

Extensive copying or publication of the thesis in whole or in part also requires the consent of the Dean of the Graduate School of the University of Kentucky.

A library that borrows this thesis for use by its patrons is expected to secure the signature of each user.

Name	Date

THESIS

Xingxing Zhang

The Graduate School

University of Kentucky

2008

STRANDED CORE TRANSFORMER LOSS ANALYSIS

THESIS

A thesis submitted in partial fulfillment of the requirements
for the degree of Master of Science in Electrical Engineering in the
College of Engineering at the University of Kentucky

By

Xingxing Zhang

Lexington, Kentucky

Director: Dr. Cai-Cheng Lu, Professor of Electrical Engineering

Lexington, Kentucky

2008

ACKNOWLEDGMENTS

The following thesis, while an individual work, benefited from the insights and direction of several people. First, my Thesis Chair, Dr. Cai-Cheng Lu, exemplifies the high quality scholarship to which I aspire. In addition, I wish to thank the complete Thesis Committee: Dr. Yuan Liao and Dr. Stephen Gedney. Each individual provided insights that guided and challenged my thinking, substantially improving the finished product.

In addition to the technical and instrumental assistance above, I received equally important assistance from family and friends. My boyfriend, Junwen Wang, provided on-going support throughout the thesis process, as well as technical assistance critical for completing the project in a timely manner. My parents, Qingyan Zhang and Mei Wu, instilled in me, from an early age, the desire and skills to obtain the Master's. Finally, I wish to thank the respondents of my study (who remain anonymous for confidentiality purposes). Their comments and insights created an informative and interesting project with opportunities for future work.

Table of Contents

List of Tables

List of Figures

List of Files

File Name: MS_Thesis_by_XingxingZhang

Type: pdf

Size: 1.25Mbytes

Chapter 1. Introduction

1.1 Background

The calculation of core loss has been considered as an important step in the designing of transformer. Power transformer core is generally made of material which has a very low iron loss. However, as the numbers of unites applied as so large, even a small loss can add up to significant amount. The iron loss is mainly caused by distortion, unequal distribution and rotating of magnetic fluxes in a core [1]. Many approaches have been studied to reduce iron loss. One of the widely used techniques is to build the core using sheet iron. Using thin sheets can significantly reduce the eddy current loss. Another new approach, which has been proposed by Busswell Energy LLC, is to use strand iron to build the cores. The fundamental benefit of using a magnetic iron core made of stranded iron in a utility transformer is the reduction in the transformer's iron loss [2].

The application of the finite element method (FEM) has brought a great advance in analytical techniques for power transformer for power loss analysis. The 3D finite element analysis has been well developed in the recent three decades to compute unknowns such as magnetic field, magnetostatic field and magnetic vector potential [2-6]. Lately, finite element method has been improved for both accuracy and efficiency. In the application of solving three-dimensional magnetostatics, the nodal scalar potential function is mixed with a face-edge formulation to obtain a more accurate result [7]. A transient edge-based vector formulation is utilized to compute the induced eddy-current losses in the rotor of a claw-pole alternator and the use of adaptive mesh optimization leads to a correct result [8]. Mesh quality can directly affect the accuracy of finite element analysis. A new mesh improvement system related to potential benefits and costs are investigated using a suite of electromagnetic benchmarks and mesh quality measures

theoretically linked to FEM accuracy [9]. The hybrid finite element method and boundary integral method is widely used for scattering and radiation problems while this method has a very slow convergence rate since the finite element matrix is ill-conditioned. The improvement of this method including the adoption of multi-frontal method makes the hybrid method converge very fast and still keeps accuracy [10].

In this thesis, our goal is to predict the iron loss of a three winding stranded core transformer with complex geometry. A commercial software Ansoft Maxwell 3D is used to compute magnetostatic field in three dimension models. However, the 3D modeling through Maxwell 3D can only model cores of transformer with uniformed materials. In this case, the B-H curve of stranded core material, which is provided by the manufacturer, need to be modified for the uniform core via two-dimensional finite element method.

In this two-dimensional finite element approach, the first order triangle elements were used with a nodal basis function. The basic field equation is vector Poisson's equation [11, 12]. We need to solve the magnetic vector potential in Poisson's equation by dividing the field region into small elements and approximate the unknown by linear equation in every element. The Dirichlet boundary condition is imposed on the mesh terminal. By the definition of magnetic vector potential, the magnetic flux density can be solved to modify the B-H curve for uniform core.

Maxwell 3D is an electromagnetic field simulation software used for the design and analysis of 3D structures. In this thesis, we used Maxwell 3D to analysis and display field distribution of 3D transformer model and output result data at selected points. The pre-processing work included core volume discretization and center points of each elements output. The post processing work is to integrate the core loss per unit volume which determined by the magnitude of B field.

1.2 Thesis structure

In this thesis, we presented a method to calculate the core loss of a three phase transformer. The main procedure of this method is as following:

1) A finite element method using nodal basis function is derived and validated for 2D magnetostatic field.
2) B-H curve for stranded core transformer modified for uniform core.
3) Using Ansoft Maxwell3D to simulate the 3D simplified transformer model. Find the magnetic flux density distribution in order to calculate the core loss.

Chapter 2. B-H curve Modification via Finite Element Method

In the process of 3D modeling using Maxwell 3D, uniform core is used to substitute stranded core. Therefore, the B-H curve which represents the material characteristics needs to be modified. In this chapter, a two-dimensional finite element approach is used to modify the B-H curve for uniform core.

2.1 Theory and formulations

2.1.1 Govern equation and weak form

The 2D magnetostatic problem has been formed in terms of the magnetic vector potential A, which defined as:

$$\nabla \times \vec{A} = \vec{B} \tag{2.1}$$

$$\nabla \cdot \vec{A} = 0 \tag{2.2}$$

It is assumed that the excitation $J = J_z \hat{z}$ which is independent of the variable z. For this excitation, the vector potential $\vec{A}$ has $\hat{z}$ component only. The govern vector Poisson equation for $\vec{A}$ can be written as:

$$\nabla \times \left(\frac{1}{\mu_r} \nabla \times \overrightarrow{A_z} \right) = \mu_0 \overrightarrow{J_z} \tag{2.3}$$

Therefore, the magnetic flux density can be calculated from $\vec{B} = \nabla \times \overrightarrow{A_z}$ [11, 12]. In the above, μ_r is the relative permeability which is a function of position.

Introducing a test function $\vec{A}_z^a$, we can derive the weak form of vector Poisson equation as,

$$F\left(\overrightarrow{A_z},\overrightarrow{A_z^a}\right)=\int_V \overrightarrow{A_z^a}\cdot\left\{\left[\nabla\times\left(\frac{1}{\mu_r}\nabla\times\overrightarrow{A_z}\right)\right]-\mu_0\overrightarrow{J_z}\right\}dV \tag{2.4}$$

Using vector identity $\vec{A}\cdot\nabla\times\vec{B}=-\nabla\cdot(\vec{A}\times\vec{B})+\vec{B}\cdot\nabla\times\vec{A}$, Equation (2.4) can be simplified in a 2D case [11],

$$F\left(\overrightarrow{A_z},\overrightarrow{A_z^a}\right)=\frac{1}{\mu_r}\int_V\nabla\times\overrightarrow{A_z^a}\cdot\nabla\times\overrightarrow{A_z}dV-\mu_0\int_V\overrightarrow{A_z^a}\cdot\overrightarrow{J_z}dV-\frac{1}{\mu_r}\oint_\Gamma\overrightarrow{A_z^a}\times\left(\nabla\times\overrightarrow{A_z}\right)\cdot\hat{n}dl \tag{2.5}$$

where $\hat{n}$ denotes the unit vector normal to Γ.

Equation (2.5) is the weak form of 2D vector Poisson equation.

2.1.2 Triangular elements

Before the derivation of finite element analysis for a 2D magnetostatic problem, a useful area coordinates (L_1,L_2,L_3) is presented below.

A convenient set of coordinates (L_1,L_2,L_3) for a triangle $(1,2,3)$ in Figure 2.1 is defined by the following linear equations in Cartesian system:

$$\begin{cases}x=L_1x_1+L_2x_2+L_3x_3\\ y=L_1y_1+L_2y_2+L_3y_3\\ 1=L_1+L_2+L_3\end{cases} \tag{2.6}$$

Every set of (L_1,L_2,L_3) corresponds to a unique set of Cartesian coordinates [13].

Solving Equation (2.6) for x and y, we have

$$\begin{cases}L_1=\dfrac{a_1+b_1x+c_1y}{2\Delta}\\ L_2=\dfrac{a_2+b_2x+c_2y}{2\Delta}\\ L_3=\dfrac{a_3+b_3x+c_3y}{2\Delta}\end{cases} \tag{2.7}$$

where,

$$\Delta = \frac{1}{2}\det\begin{vmatrix} 1 & x_1 & y_1 \\ 1 & x_2 & y_2 \\ 1 & x_3 & y_3 \end{vmatrix} = \text{area of trangle123}$$

and

$$\begin{cases} a_1 = x_2 y_3 - x_3 y_2 \\ b_1 = y_2 - y_3 \\ c_1 = x_3 - x_2 \end{cases} \tag{2.8}$$

$$\begin{cases} a_2 = x_3 y_1 - y_3 x_1 \\ b_2 = y_3 - y_1 \\ c_2 = x_1 - x_3 \end{cases} \tag{2.9}$$

$$\begin{cases} a_3 = x_1 y_2 - y_1 x_2 \\ b_3 = y_1 - y_2 \\ c_3 = x_2 - x_1 \end{cases} \tag{2.10}$$

Based on the above definition, we observe that when point P on edge 23, $L_1 = 0$; if it is on vertex 1, then $L_1 = 1$.

When point P on edge 13, $L_2 = 0$; if it is on vertex 2, then $L_2 = 1$.

When point P on edge 12, $L_3 = 0$; if it is on vertex 3, then $L_3 = 1$.

The major advantage of triangular elements is that they can be used in problems with irregular geometries. In finite element procedure, triangular mesh is widely adopted and area coordinates are used to represent both linear and nonlinear local functions.

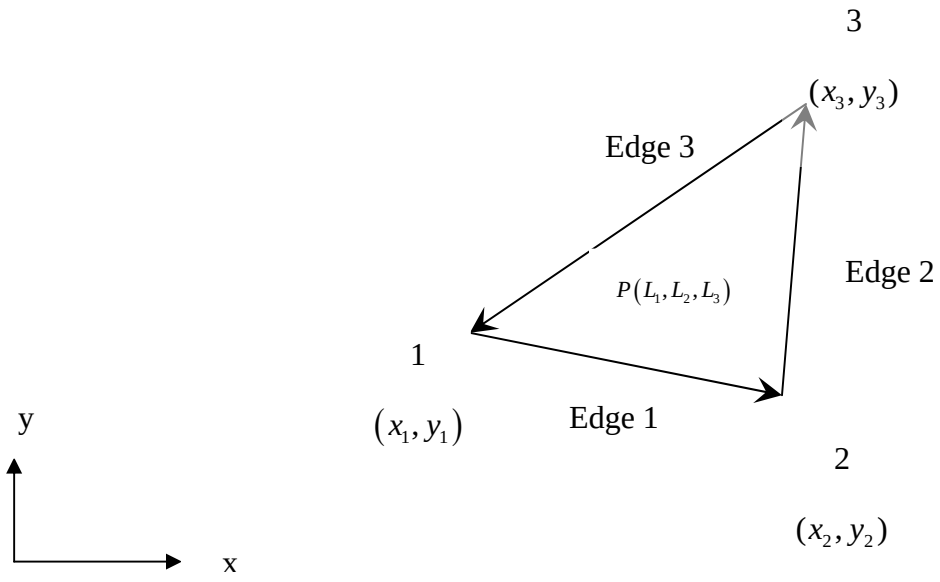

Figure 2.1. Parameters of a typical triangle

2.1.3 Linear interpolation function of magnetic potential

In a triangular element, the magnetic potential component $A_z(x,y)$ at any point can be approximated by the linear interpolation function defined at every vertex.

In the triangle of Figure 2.1, the magnetic potential $A_z(x,y)$ can be approximated as:

$$A(x,y) = a + bx + cy \tag{2.11}$$

If the potential has values of A_1, A_2 and A_3 at the vertices 1, 2 and 3 respectively, then we apply Equation (2.11) to the three vertices to obtain,

$$\begin{cases} A_1 = a + bx_1 + cy_1 \\ A_2 = a + bx_2 + cy_2 \\ A_3 = a + bx_3 + cy_3 \end{cases} \tag{2.12}$$

This will allow us to solve for the expansion coefficients (a,b,c). The results are listed as follows,

$$\begin{cases} a = \dfrac{1}{2\Delta}\left(a_1A_1 + a_2A_2 + a_3A_3\right) \\ b = \dfrac{1}{2\Delta}\left(b_1A_1 + b_2A_2 + b_3A_3\right) \\ c = \dfrac{1}{2\Delta}\left(c_1A_1 + c_2A_2 + c_3A_3\right) \end{cases} \tag{2.13}$$

Pluging Equation (2.13) in Equation (2.11), we get,

$$A(x,y) = \frac{1}{2\Delta}\sum_{i=1}^{3}\left(a_i + b_ix + c_iy\right)A_i \tag{2.14}$$

In terms of area coordinates, Equation (2.14) becomes

$$A(x,y) = \sum_{i=1}^{3} L_iA_i \tag{2.15}$$

Thus, we obtained the linear representation of the unknown potential using its values at the vertices of triangles.

2.1.4 Local element calculation

From Equation (2.15), nodal basis expansion in each element can be expected in such a form:

$$\vec{A}_z^e = \sum_{i=1}^{3} C_i L_i(x,y)\hat{z} \text{ and } \vec{A}_z^{ae} = \sum_{j=1}^{3} L_j(x,y)\hat{z} \tag{2.16}$$

where C_i is the unknown coefficient which needs to be determined.

Now, we discretize Equation (2.5) on each triangle. The triangle index "e" is ignored for some quantities for simplicity.

Define

$$S_{ij} = \int_V \frac{1}{\mu_r}\left(\nabla \times L_j(x,y)\hat{z}\right)\cdot\left(\nabla \times L_i(x,y)\hat{z}\right)dV \tag{2.17}$$

$$B_j = \int_V L_j(x,y)\hat{z}\cdot\vec{J}_z dV \tag{2.18}$$

$$\Gamma_{ij} = \int_\Gamma \frac{1}{\mu_r} L_j(x,y)\hat{z}\times\left(\nabla \times L_i(x,y)\hat{z}\right)\cdot\hat{n}dl \tag{2.19}$$

where $\hat{n}$ denotes the unit vector normal to Γ.

Then, function $F\left(\vec{A}_z^e, \vec{A}_z^{ae}\right)$ can be expanded in local element as

$$F\left(\vec{A}_z^e, \vec{A}_z^{ae}\right) = \sum_{i=1}^{3}\sum_{j=1}^{3}\left(C_i S_{ij} - \mu_0 B_j - C_i\Gamma_{ij}\right) \tag{2.20}$$

In the following part, we will discuss each matrix respectively.

1) S matrix calculation

Using some vector identities, S_{ij} can be simplified as

$$
\begin{aligned}
S_{ij} &= \int_V \frac{1}{\mu_r}\left(\nabla \times L_j\left(x,y\right)\hat{z}\right)\cdot\left(\nabla \times L_i\left(x,y\right)\hat{z}\right)dV \\
&= \int_V \frac{1}{\mu_r}\left(\frac{\partial}{\partial y}L_j\hat{x} - \frac{\partial}{\partial x}L_j\hat{y}\right)\cdot\left(\frac{\partial}{\partial y}L_i\hat{x} - \frac{\partial}{\partial x}L_i\hat{y}\right)dV \\
&= \int_V \frac{1}{\mu_r}\left(\frac{\partial}{\partial y}L_j\frac{\partial}{\partial y}L_i + \frac{\partial}{\partial x}L_i\frac{\partial}{\partial x}L_j\right)dV
\end{aligned}
\tag{2.21}
$$

By the definition of area coordinates, the differential operation can be calculated as

$$
\frac{\partial}{\partial y}L_i = \frac{\partial}{\partial y}\frac{a_i + b_i x + c_i y}{2\Delta} = \frac{1}{2\Delta}c_i \quad \text{and} \quad \frac{\partial}{\partial x}L_i = \frac{\partial}{\partial x}\frac{a_i + b_i x + c_i y}{2\Delta} = \frac{1}{2\Delta}b_i
$$

In the same way, we have,

$$
\frac{\partial}{\partial y}L_j = \frac{1}{2\Delta}c_j \ \text{ and } \ \frac{\partial}{\partial x}L_j = \frac{1}{2\Delta}b_j
$$

Imposing the results in equation (2.21),

$$
\begin{aligned}
S_{ij} &= \int_V \left(\frac{1}{2\Delta}c_i\frac{1}{2\Delta}c_j + \frac{1}{2\Delta}b_i\frac{1}{2\Delta}b_j\right)\frac{1}{\mu_r}dV \\
&= \int_{L_2=0}^{1}\int_{L_1=0}^{1-L_2}\left(\frac{1}{2\Delta}c_i\frac{1}{2\Delta}c_j + \frac{1}{2\Delta}b_i\frac{1}{2\Delta}b_j\right)\frac{1}{\mu_r}\sqrt{g}\,dL_1dL_2
\end{aligned}
$$

where $\sqrt{g} = 2\Delta$, and Δ is the area of the triangle

Then,

$$
S_{ij} = \frac{1}{\mu_r}\left(\frac{1}{4\Delta}c_i c_j + \frac{1}{4\Delta}b_i b_j\right) \tag{2.22}
$$

2) B **matrix calculation**

Similarly, the result of B matrix calculation can be written as

$$
\begin{aligned}
B_j &= \int_V L_j\left(x,y\right)\hat{z}\cdot\vec{J}_z dV = J\int_V L_j dV \\
&= J\int_{L_2=0}^{1}\int_{L_1=0}^{1-L_2} L_j\sqrt{g}\,dL_1dL_2 \\
&= J\frac{1}{6}\sqrt{g} = J\frac{\Delta}{3}
\end{aligned}
\tag{2.23}
$$

In the above, J is the excitation current at the center of the triangles.

3) Γ matrix calculation

By definition,

$$C_i\Gamma_{ij} = \int_{\Gamma} \frac{1}{\mu_r} L_j(x,y)\hat{z} \times \left(\nabla \times C_i L_i(x,y)\hat{z}\right) \cdot \hat{n} dl$$

Using vector identities, $\nabla \times (ab) = a\nabla \times b - b \times \nabla a$ and $a \times (b \times c) = (a \cdot c)b - (a \cdot b)c$

we have,

$$\begin{aligned} \nabla \times \left(C_i L_i \hat{z}\right) &= C_i L_i \left(\nabla \times \hat{z}\right) - \hat{z} \times \nabla C_i L_i \\ &= C_i \nabla L_i \times \hat{z} \end{aligned} \tag{2.24}$$

Thus,

$$\begin{aligned} C_i\Gamma_{ij} &= \int_{\Gamma} \frac{1}{\mu_r} L_j \hat{z} \times (C_i \nabla L_i \times \hat{z}) \cdot \hat{n} dl \\ &= \int_{\Gamma} \frac{1}{\mu_r} \left[(L_j \hat{z} \cdot \hat{z}) C_i \nabla L_i - (L_i \hat{z} \cdot C_i \nabla L_i) \right] \cdot \hat{n} dl \\ &= \int_{\Gamma} \frac{1}{\mu_r} L_j \nabla C_i L_i \cdot \hat{n} dl \end{aligned} \tag{2.25}$$

In the above, we have applied the fact the ∇L is in x-y plane where $\hat{z} \cdot \nabla L = 0$.

For every triangular mesh,

$$\sum_{i=1}^{3} C_i\Gamma_{ij} = \int_{\Gamma} \frac{1}{\mu_r} L_j \frac{\partial A_z^e}{\partial n} dl \tag{2.26}$$

An example is given in Figure 2.2. Two adjacent triangular elements were used for illustration.

In triangle 1,

$$\sum_{i=1}^{3} C_i\Gamma_{ij} = \frac{1}{\mu_r^{e1}} \frac{\partial A_z^{e1}}{\partial n} \left(\int_{\text{node1}}^{\text{node2}} L_j dl + \int_{\text{node2}}^{\text{node3}} L_j dl + \int_{\text{node3}}^{\text{node1}} L_j dl \right) \tag{2.27}$$

In triangle 2,

$$\sum_{i=1}^{3} C_i\Gamma_{ij} = \frac{1}{\mu_r^{e2}} \frac{\partial A_z^{e2}}{\partial n} \left(\int_{\text{node2}}^{\text{node4}} L_j dl + \int_{\text{node3}}^{\text{node2}} L_j dl + \int_{\text{node4}}^{\text{node3}} L_j dl \right) \tag{2.28}$$

For two adjacent triangle mesh which share a same edge, at the interface, the magnetic potential satisfies [12]

$$A_z^{e1} = A_z^{e2} \quad \text{and} \quad \frac{1}{\mu_r^{e1}} \frac{\partial A_z^{e1}}{\partial n} = \frac{1}{\mu_r^{e2}} \frac{\partial A_z^{e2}}{\partial n}.$$

Thus, the middle terms of the right-hand side in Equation (2.27) and Equation (2.28) cancelled. Therefore, Γ matrix can be cancelled at all interior edges. We will discuss the outer boundary condition later.

4) Magnetic flux density calculation

From Equation (2.1), B can be expanded in local element as,

$$\begin{aligned} B^e &= \sum_{i=1}^{3} \nabla \times \left(C_i L_i \right) \hat{z} \\ &= \sum_{i=1}^{3} C_i \left(\frac{\partial}{\partial y} L_i \hat{x} - \frac{\partial}{\partial x} L_i \hat{y} \right) \\ &= \sum_{i=1}^{3} C_i \frac{1}{2\Delta} \left(c_i \hat{x} - b_i \hat{y} \right) \end{aligned} \tag{2.29}$$

The weak form for local element Equation (2.20) can be simplified as:

$$F\left(\vec{A}_z^e, \vec{A}_z^{ae} \right) = \sum_{i=1}^{3} \sum_{j=1}^{3} \left(C_i S_{ij} - \mu_0 B_j \right) = C_{lem} S_{lem} - \mu_0 B_{lem}$$

To minimize the equation, we set $F = 0$. This leads to $C_{lem} = \mu_0 B_{lem} S_{lem}^{-1}$.

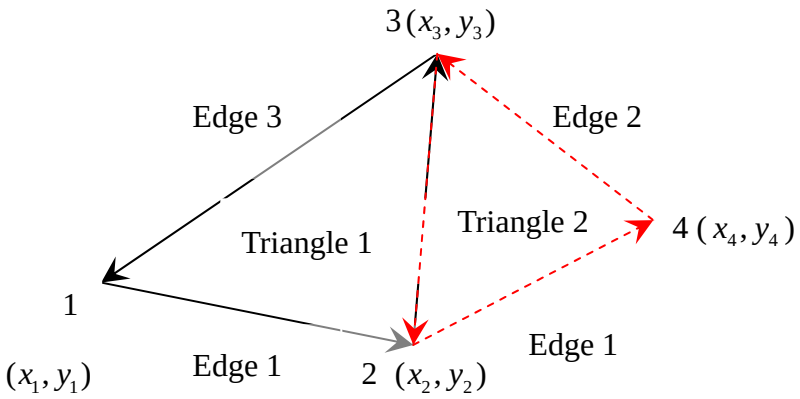

Figure 2.2. Example to illustrate the integration on the interior boundary

2.1.5 Boundary Condition

There are several absorbing boundary conditions to be applied for mesh truncation. When the boundary is far enough to the transformer model, the Dirichlet Boundary Condition,

$$A(x, y) = 0 \tag{2.30}$$

on the outer boundary can yield an accurate solution.

2.2 Validation of finite element method

2.2.1 Ampere's circuital law

Ampere's circuital law states that the line integral of H about any closed path is exactly equal to the direct current enclosed by that path [14],

$$\oint H \cdot dL = I \tag{2.31}$$

The magnetic flux density is related to H by

$$B = \mu_0 \mu_r \mathrm{H} \tag{2.32}$$

In the govern vector Poisson Equation $\nabla \times \left(\frac{1}{\mu_r} \nabla \times \overrightarrow{A_z} \right) = \mu_0 \overrightarrow{J_z}$, $\overrightarrow{J_z}$ denotes the electric current density with the unit $\mathrm{A/m^2}$. If $\overrightarrow{J_z}$ is uniformly distributed, the total current I can be calculated from $\overrightarrow{J_z} \cdot \Delta$, where Δ is the area containing $\overrightarrow{J_z}$.

We will test the FEM program with three test cases and compare the result with the exact H value computed by Ampere's circuital law.

2.2.2 Test case 1

The first case is a conductor of circular cross section with a radius $a = 0.1\mathrm{m}$ which has a relative permeability $\mu_r = 1$. A current density $J = 1\,\mathrm{A/m^2}$ is imposed on it. The background mesh is terminated at a circle of radius $g = 1.2\mathrm{m}$. The geometry is shown in Figure 2.3.

The exact H can be calculated as

$$H = \frac{J\pi^2 r}{2\pi r} = \frac{J\pi}{2}, \quad r < a, \tag{2.33}$$

$$H = \frac{J\pi^2 a}{2\pi r} = \frac{J\pi a}{2r}, \quad r \geq a, \tag{2.34}$$

Using the finite element program, H is calculated at fixed angles of $0^\circ, 45^\circ$ and 90°, respectively. Figure 2.4 is the comparison of results of FEM and the exact H value. Figure 2.5 and Figure 2.6 show the mesh plot [15]. The figures show that the results calculated by FEM agree well with the exact results.

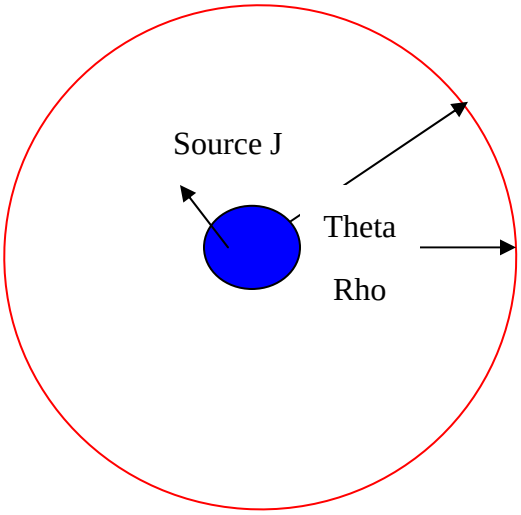

Figure 2.3. Case 1 geometric model

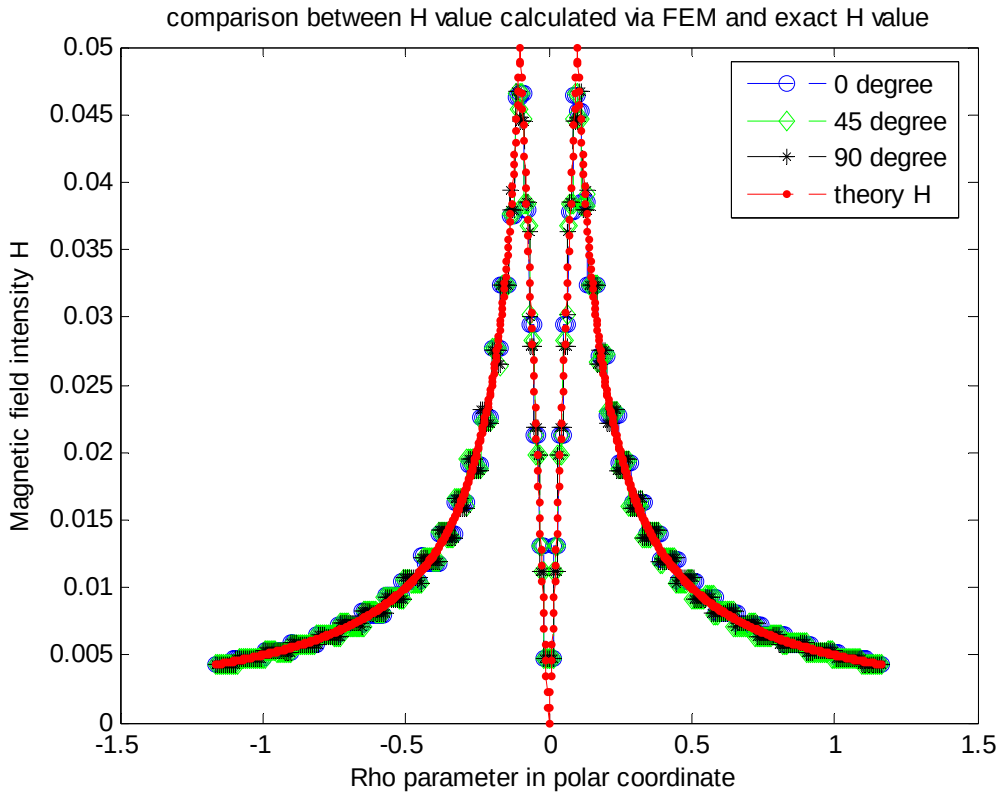

Figure 2.4. Comparison between H value calculated via FEM and exact result for Case 1

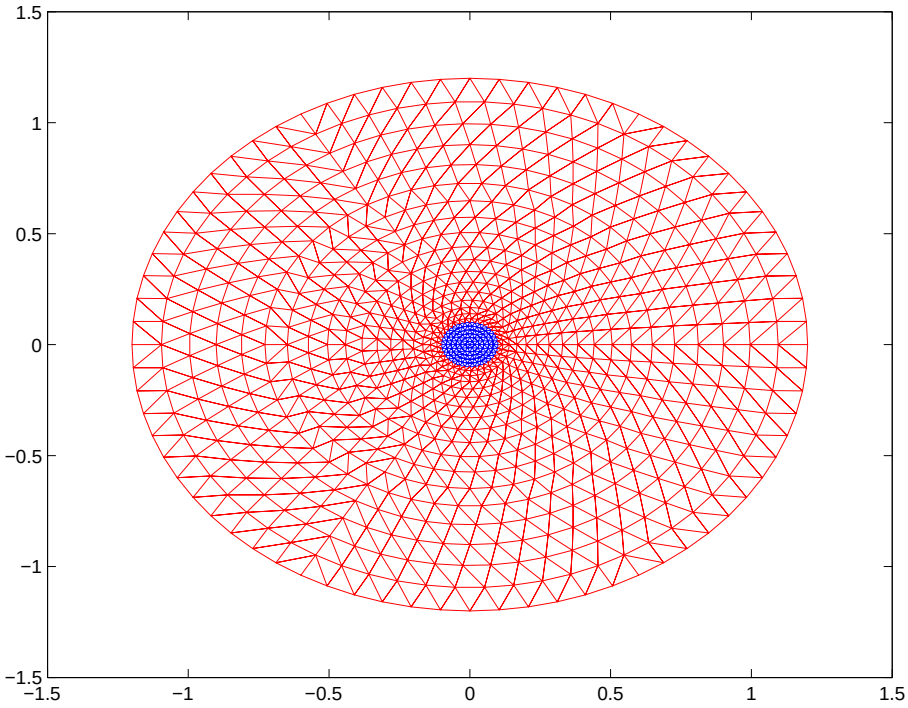

Figure 2.5. Mesh plot for Case 1

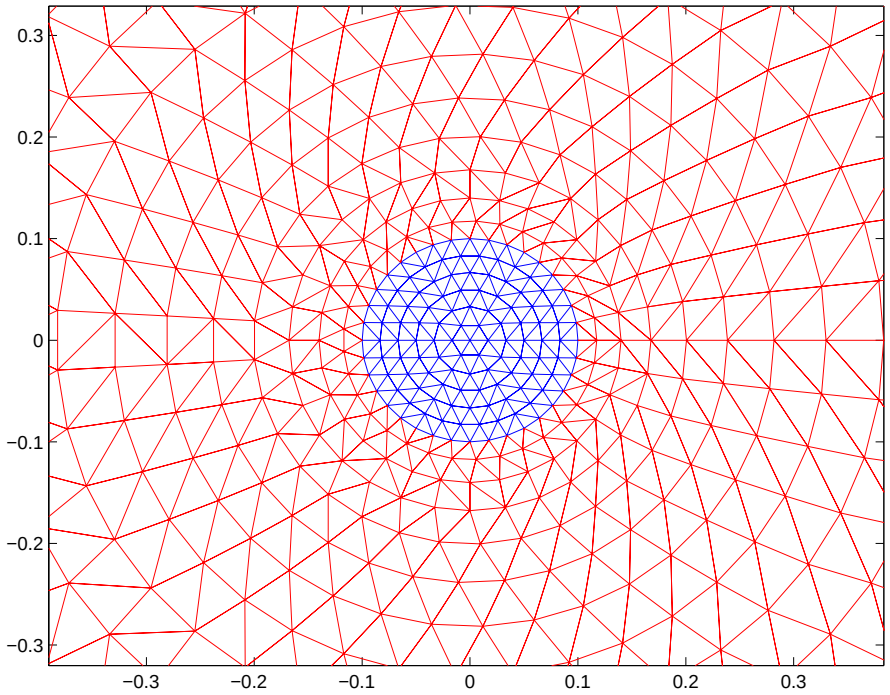

Figure 2.6. Detail mesh plot of Case 1

2.2.3 Test case 2

The second case is a circle cross section of a conductor with a radius $a = 0.1m$ which has a relative permeability $\mu_r = 1$. A current density $J = 1\,\text{A/m}^2$ is imposed on it. A material which has a relative permeability $\mu_r = 900$ surrounds the source with a radius $b = 0.2\,\text{m}$. The background is filled of air with a radius $g = 1\text{m}$ which has a relative permeability $\mu_r = 1$. The geometry is shown in Figure 2.7.

The exact H can be calculated in the same way as in case 1.

The finite element program calculated H at fixed angles of $0^\circ, 45^\circ$ and 90° respectively. Figure 2.8 is the comparison of results of FEM and the exact H value. Figure 2.9 and Figure 2.10 show the mesh plot.

The figures show that the results calculated by FEM agree well with the exact results

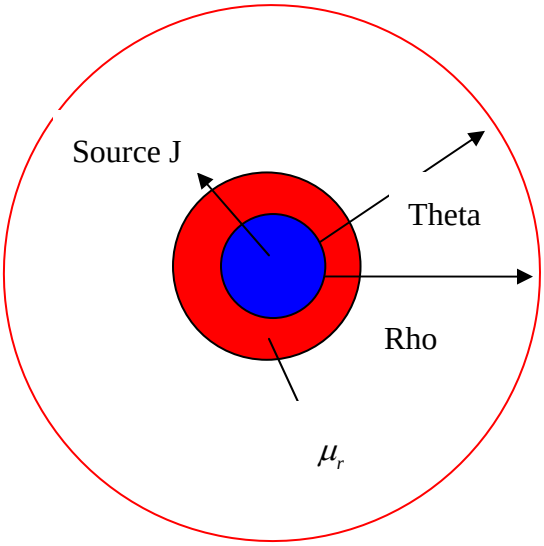

Figure 2.7. Geometric model of Case 2

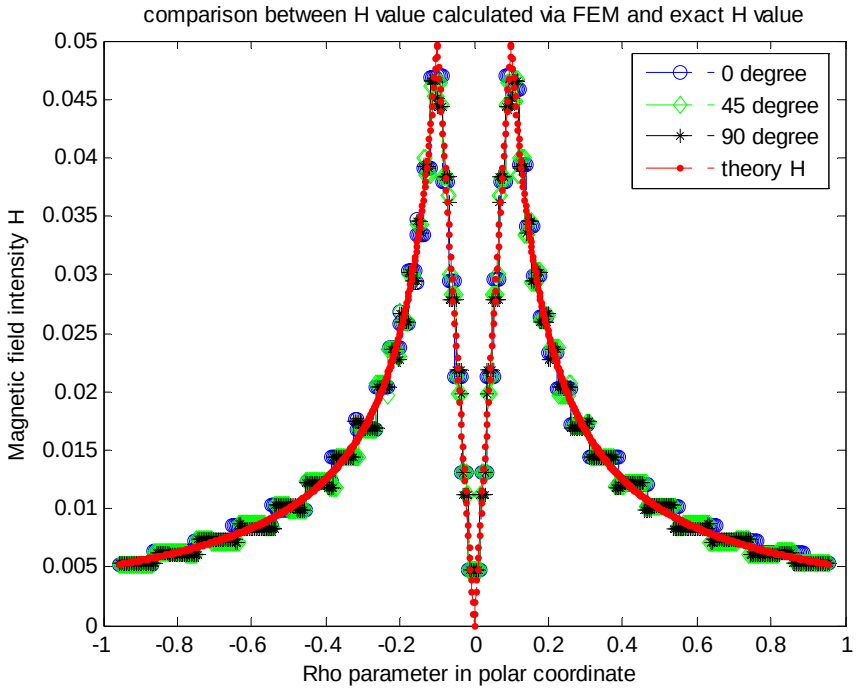

Figure 2.8. Comparison between H value calculated via FEM and exact H value in Case 2

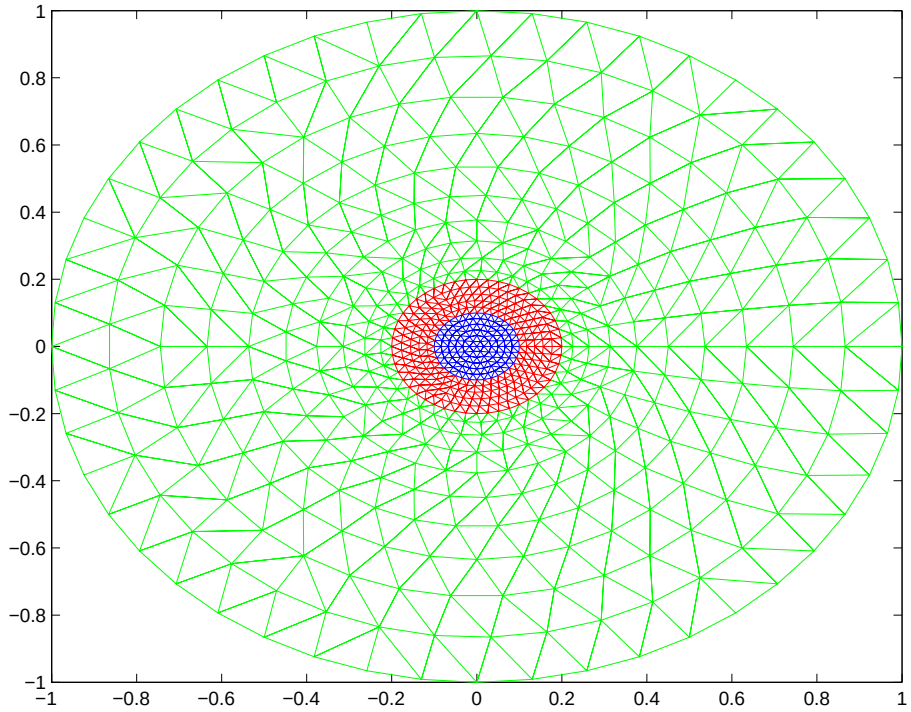

Figure 2.9. Mesh plot for Case 2

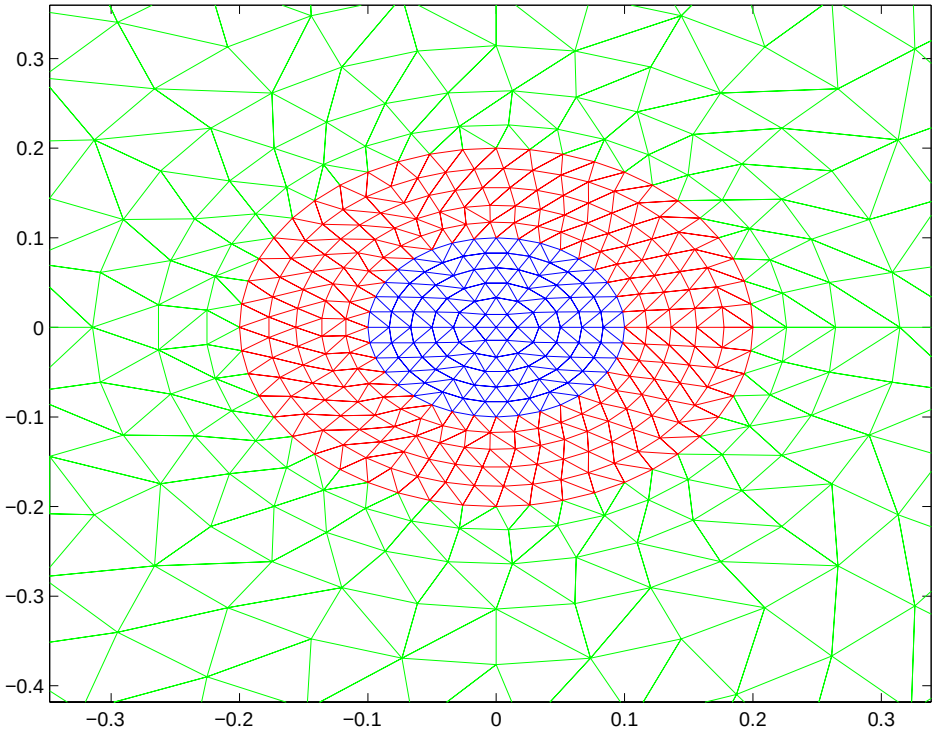

Figure 2.10. Detailed mesh plot for Case 2

2.2.4 Test case 3

The third case is a ring cross section of a conductor with an inner radius $a = 0.1\text{m}$ and outer radius $b = 0.2\text{m}$ which has a relative permeability $\mu_r = 1$. A current density $J = 1\text{A/m}^2$ is imposed on it. A material which has a relative permeability $\mu_r = 900$ surrounds the source with a radius $c = 0.24\text{m}$. The background is filled of air with a radius $g = 1.2\text{m}$ which has a relative permeability $\mu_r = 1$. The geometry is shown in Figure 2.11.

The exact H can be calculated from

$$H = 0, \quad r < a, \tag{2.35}$$

$$H = \frac{\pi\left(r^2 - a^2\right)J}{2\pi r} = \frac{\left(r^2 - a^2\right)J}{2r}, \quad a \le r < b, \tag{2.36}$$

$$H = \frac{\pi\left(b^2 - a^2\right)J}{2\pi r} = \frac{\left(b^2 - a^2\right)J}{2r}, \quad r \ge b, \tag{2.37}$$

The finite element program calculated H at fixed angles of $0^\circ, 45^\circ$ and 90° respectively. Figure 2.12 is the comparison of results of FEM and the exact H value. Figure 2.13 and Figure 2.14 show the mesh plot.

From Figure 2.12, we can see that the results calculated via FEM match well with the exact results.

Through testing three cases with regular geometry which have exact results, the algorithm and program of this 2D finite element method are demonstrated accurate to solve magnetostatic field. In the next section, this method will be applied on two models with different transformer core structures.

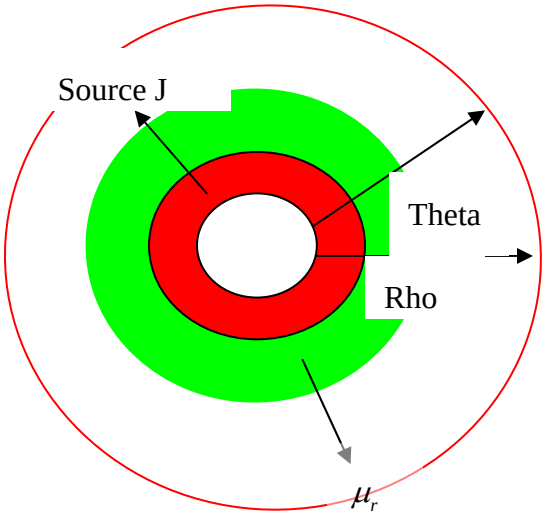

Figure 2.11. Geometric model of Case 3

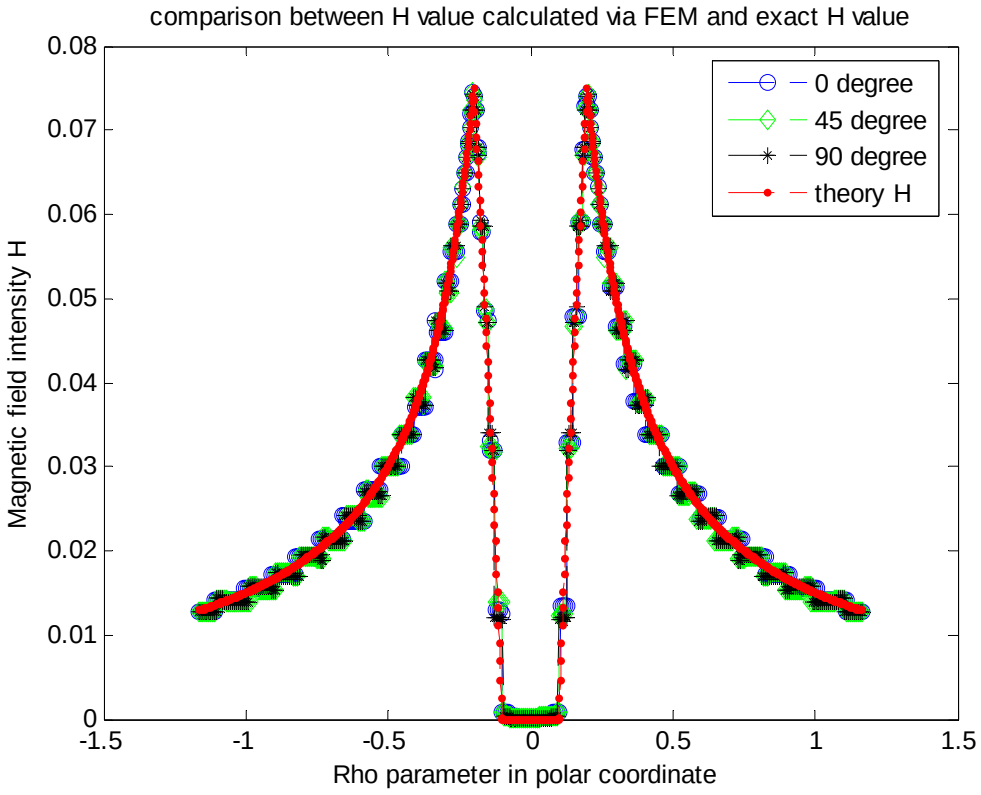

Figure 2.12. Comparison between H value calculated via FEM and exact H value in Case 3

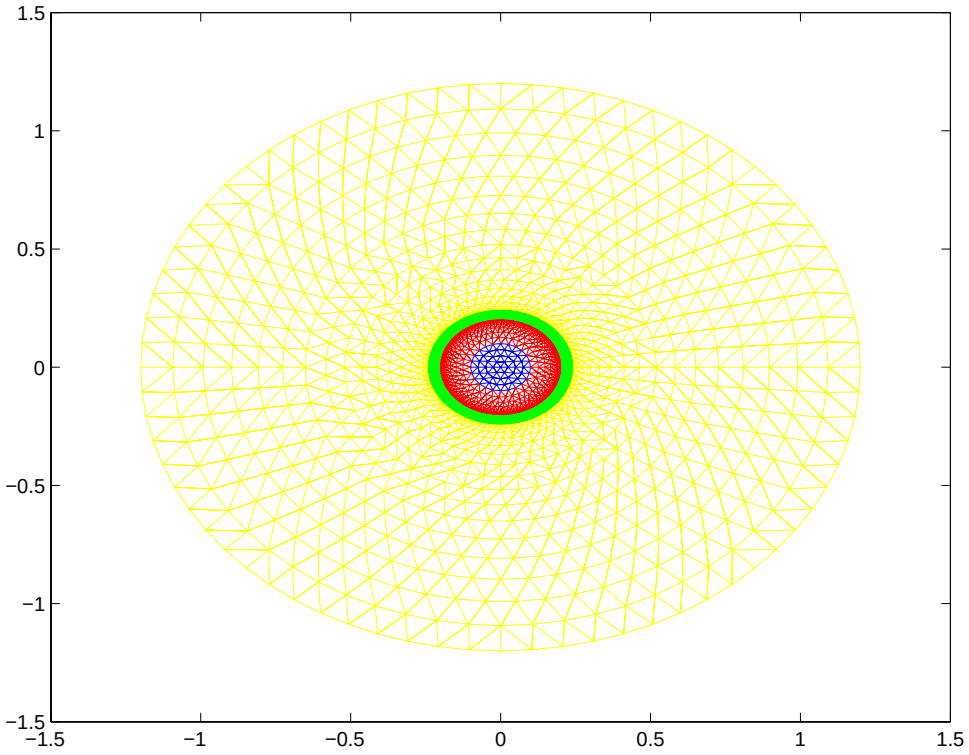

Figure 2.13. Mesh plot for Case 3

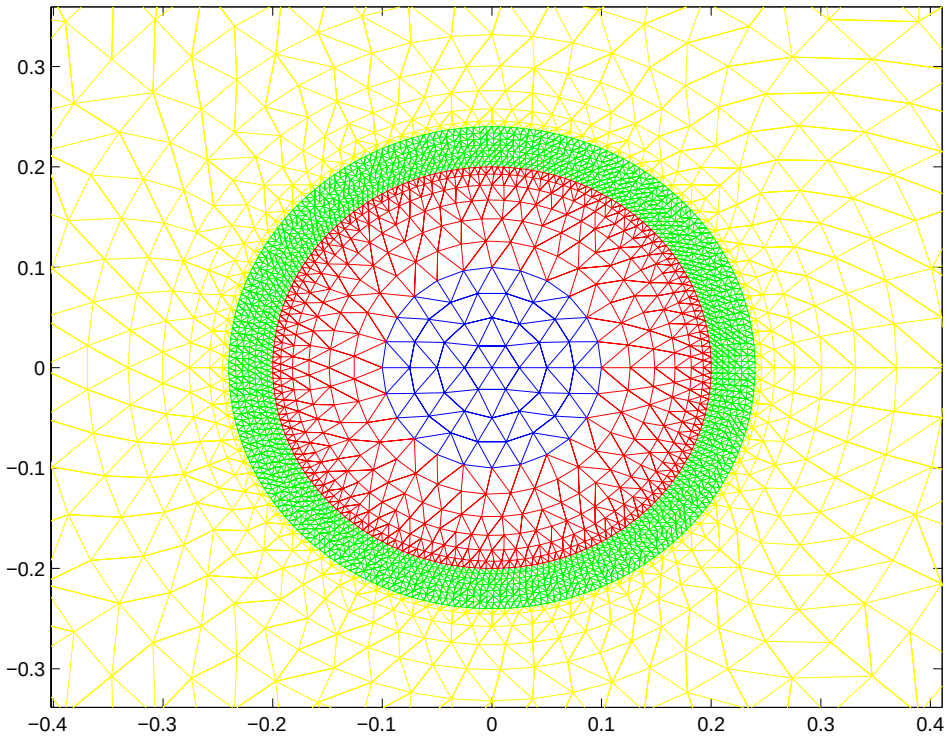

Figure 2.14. Detailed mesh plot for Case 3

2.3 B-H curve Modification

In order to predict accurate core loss for a transformer, a simple but accurate transformer model including non-linear B-H characteristics, external exciting circuit, and core loss per pound, must be available. In our case, the stranded core model is hard to model and simulate by software such as Maxwell 3D. Then, an equivalent but simple model is necessary to build. In the following part, transformer core with uniform distributed material will replace the stranded core in the simulation of core loss analysis. For an accurate result, the B-H curve needs to be modified for a uniform core transformer.

2.3.1 B field distribution in both stranded core and uniform core models

The stranded core mesh plot is shown in Figure 2.15. The source area in the upper part of the model is imposed with a current density of $J_1 = 1\,\mathrm{A/m^2}$ while the other source area in the lower part is imposed with a current density of $J_2 = -1\,\mathrm{A/m^2}$. The material between source areas denotes the stranded core. The small gaps between core sections and whole background are filled with air.

Figure 2.16 is the mesh plot for the simplified uniform core model. The source and background are the same as the stranded core model. The material of core between source areas is uniform distributed as shown in detailed mesh plot.

We start with a $\mu_r = 100$ imposed on both the stranded core and uniform core elements. Figure 2.17 and Figure 2.18 show the result of B field distribution in a patch plot view in the center core area.

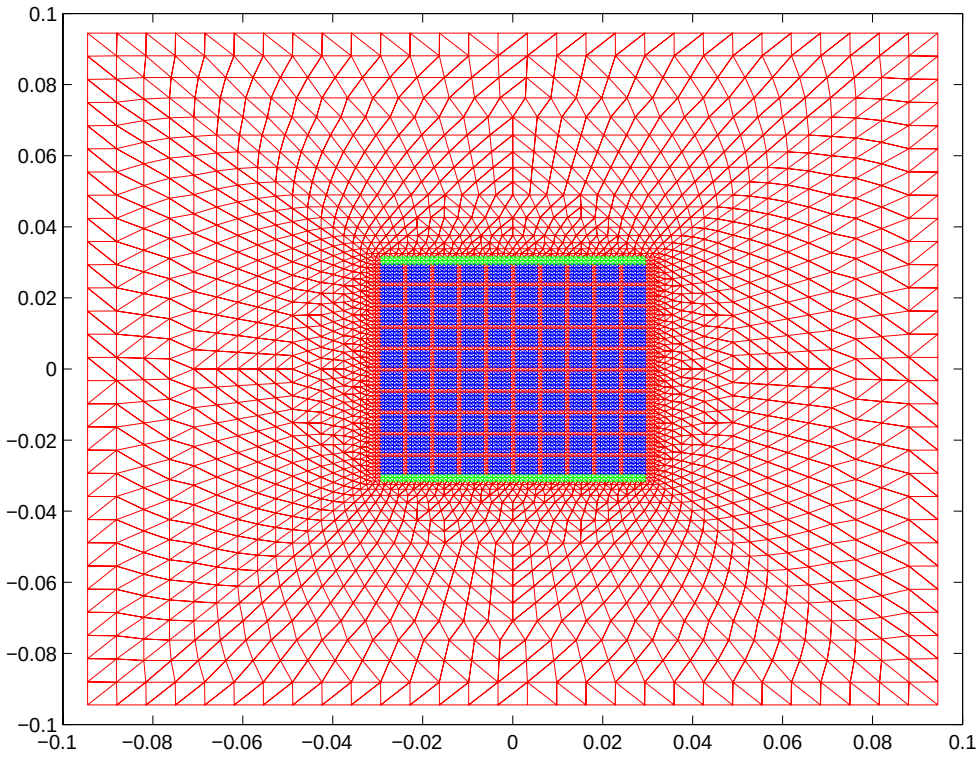

(a). Mesh plot for the stranded core model

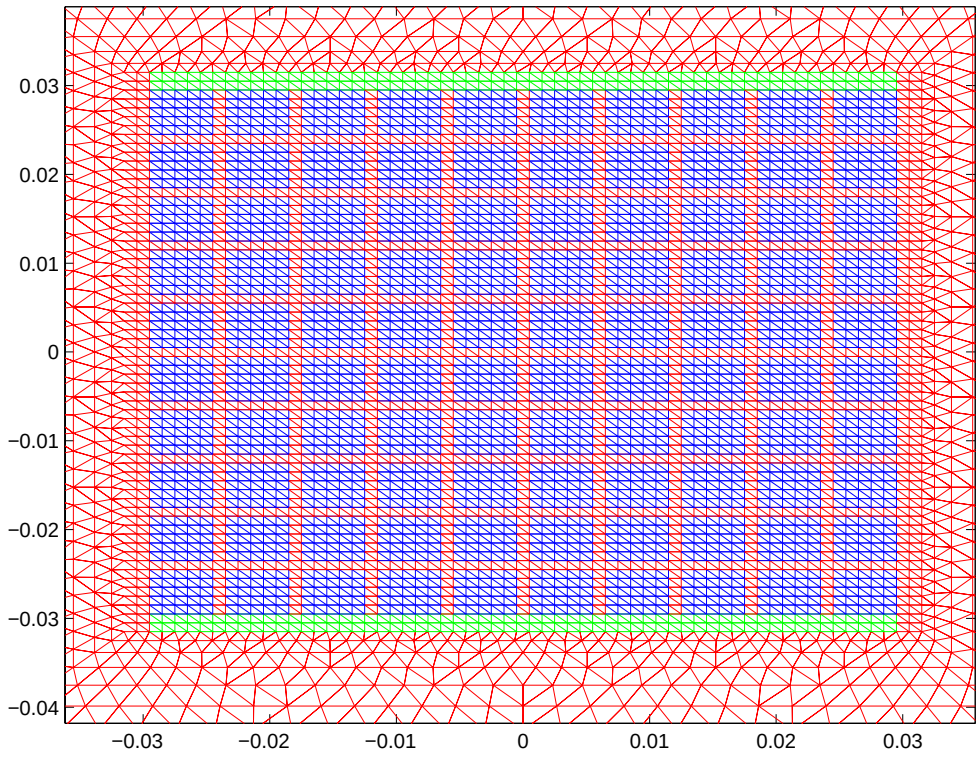

(b). Detailed mesh plot for stranded core model

Figure 2.15. Mesh plot and detailed mesh plot for the stranded core model

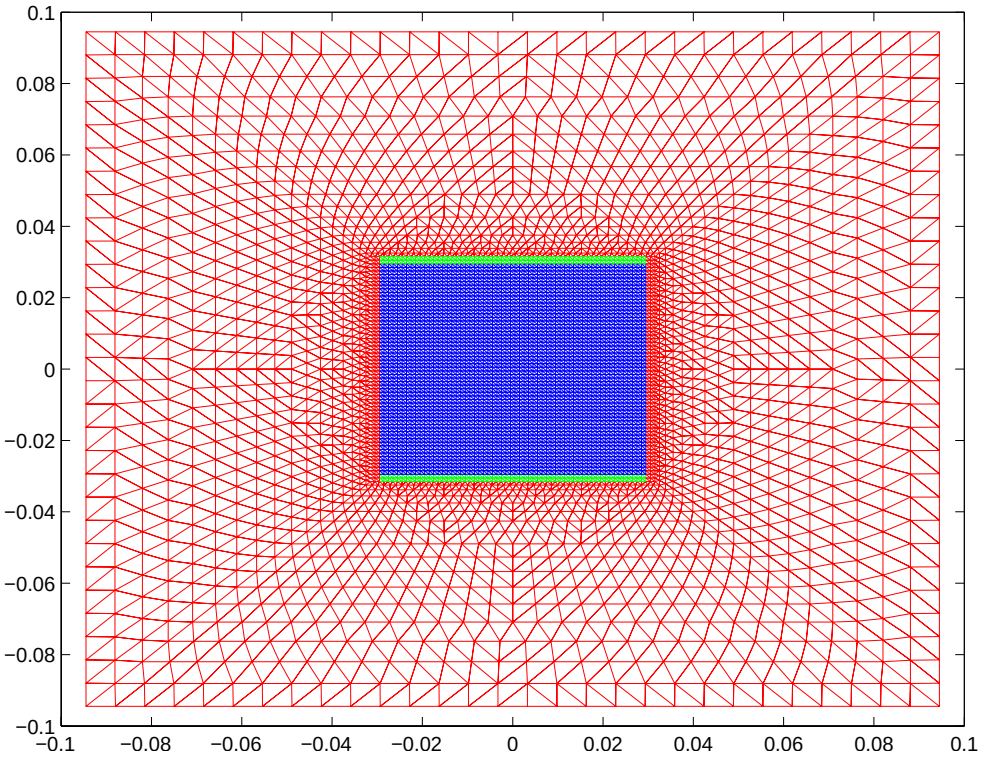

(a). Mesh plot for the uniform core model

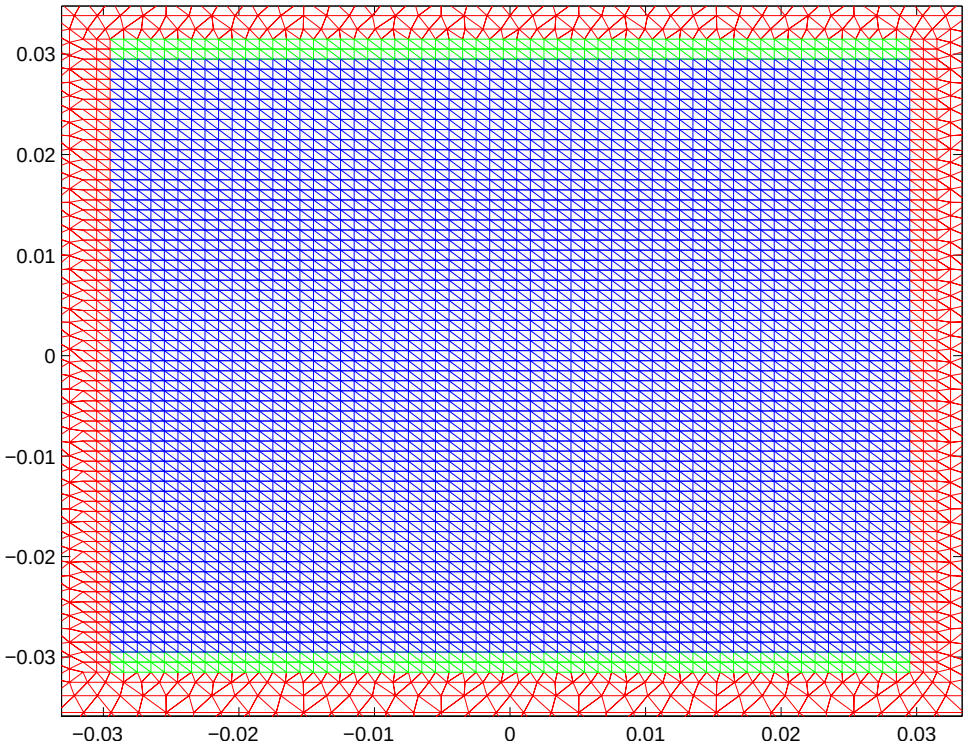

(b). Detailed mesh plot for the uniform core model

Figure 2.16. Mesh plot and detailed mesh plot for the uniform core model

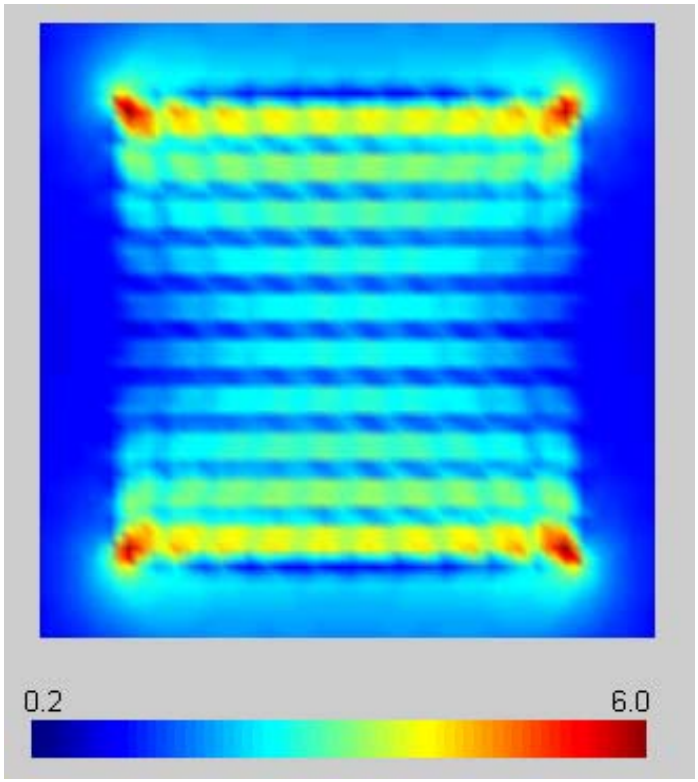

Figure 2.17. B field distribution for stranded core model

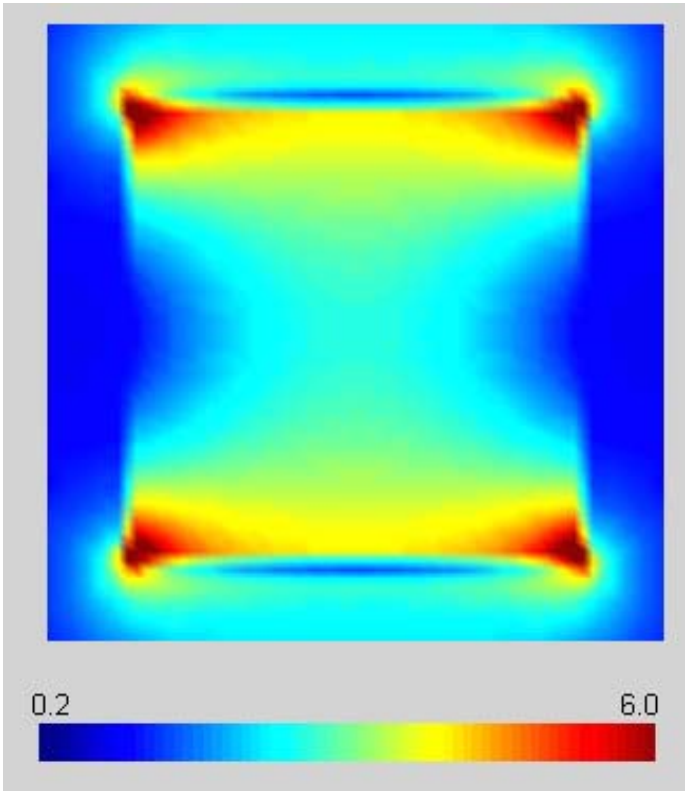

Figure 2.18. B field distribution for uniform core model

2.3.2 B-H curve modification

Table 2.1 shows the B-H curve supplied by manufacturers which obtained from measuring the stranded core transformer. Since the model has been simplified as a uniform distributed core transformer, the original B-H curve is no longer applicable to the new model. We need to modify the curve based on the results of B field calculation via finite element method.

Same mesh was applied to the model of stranded core and the model of uniform core. We calculate the error of B when relative permeability is fixed for the mesh elements in the core area of stranded core model using

$$B_{error} = \frac{\sum_{i=1}^{N} \left| B_{ui} - B_{si} \right|}{N} \tag{2.38}$$

where N denotes the total number of elements in the core area of stranded core. B_{ui} and B_{si} represent the magnetic flux density of uniform core and the magnetic flux density of stranded core in the $i-th$ element respectively.

Based on Equation (2.38), we calculate the error of B between stranded core and uniform core when relative permeability changes. Figure 2.19, Figure 2.20 and Figure 2.21 respectively show that when the relative permeability of stranded core is 150, 300 and 1000, the error of B between stranded core and uniform core. The test results are in Table 2.2, Table 2.3 and Table 2.4 respectively.

Then, we calculate B average for both stranded core and uniform core model using

$$B_{avg} = \frac{\sum_{i=1}^{N} B_i \cdot \Delta_i}{\sum_{i=1}^{N} \Delta_i} \tag{2.39}$$

where N denotes the total number of elements in the core area, B_i and Δ_i represent the magnetic flux density and area of the $i-th$ element respectively.

We change the value of μ_r for stranded core model and recalculate B_{avg}. Table 2.5 lists the test values of μ_r and the corresponding B_{avg} for the stranded core.

In the same way, Table 2.5 is the test values μ_r and the corresponding B_{avg} for the uniform core.

The B_{avg} - μ_r curves for stranded core model and uniformed core model are shown in Figure 2.22. For the purpose of transformer design, we also test μ_r and the corresponding B_{avg} for stranded core with a smaller gap and uniform core in the same mesh discretization.. We can see that B_{avg} is a fixed value when μ_r going to infinite. We will explain this phenomenon by introducing the generation of static magnetic fields [16, 17].

The basic laws of magnetostatics are

$$\nabla \cdot B = 0 \tag{2.40}$$

$$\nabla \times H = J \tag{2.41}$$

Considering a surface S which enclosed by a path C, we can operate surface integral of Equation (2.41) over S.

$$\int_s \nabla \times H ds = \int_s J ds \tag{2.42}$$

By applying Stokes' theorem to Equation (2.42), we have

$$\oint_c H dl = \int_s J ds = I \tag{2.43}$$

Equation (2.43) often states as Ampere's circuit law.

Apply Equation (2.43) to our 2D core model, we can get,

$$\frac{B_0 l_0}{\mu_0} + \frac{B_1 l_1}{\mu_r \mu_0} = J * area \tag{2.44}$$

where B_0 denotes the magnetic flux density in the air and coil. B_1 denotes the magnetic flux density in core. l_0 is the path length in the air and coil. l_1 is the path length in the core.

If the relative permeability is infinite, Equation (2.44) becomes

$$\frac{B_0 l_0}{\mu_0} = J * \text{area} \tag{2.45}$$

Thus, B_{avg} is a fixed value.

Provided with the test data, the B-H curve can be calculated through algorithm involving Fourier series and finite element analysis iteration [18]. The initial value of the iteration is fixed on the B value when relative permeability goes infinitely. The difference of $B_{\mu_r=\infty}$ between stranded core and uniform core is 2.7065×10^{-10}. When the gap size reduces to $\frac{5}{6}$ of the original gap size, the difference of $B_{\mu_r=\infty}$ between stranded core and uniform core reduces to 1.8800×10^{-10} as we expected. In our modeling, based on the original B-H curve for stranded core transformer, we can adjust the original B-H curve proportional to the values of B_{avg} when μ_r is infinite. Figure 2.24 shows the original B-H curve for stranded core transformer and the modified B-H curve for uniform core model.

The next chapter shows the Maxwell 3D simulation using the modified B-H curve and the results of iron loss prediction.

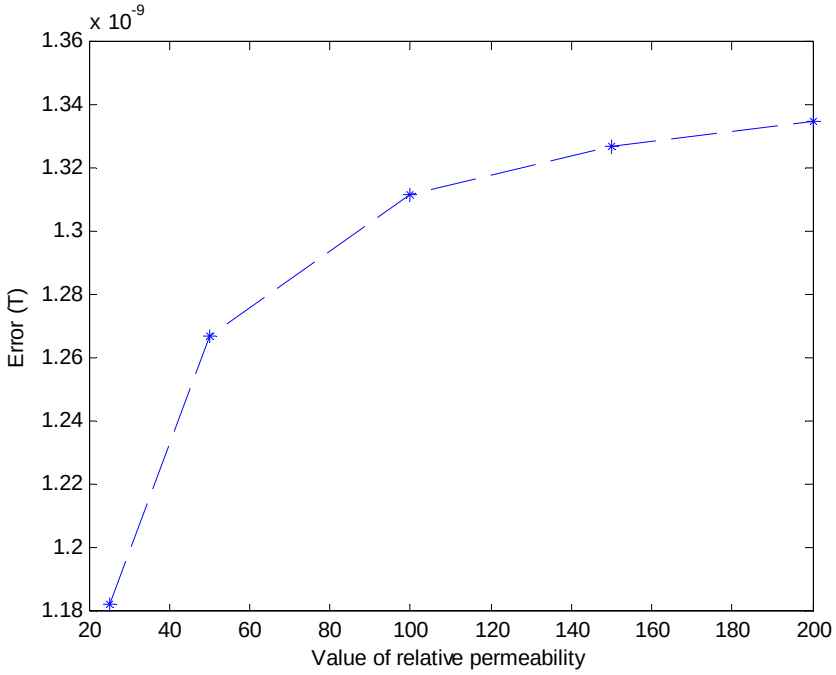

Figure 2.19. B error between stranded core with μ_r =150 and uniform core

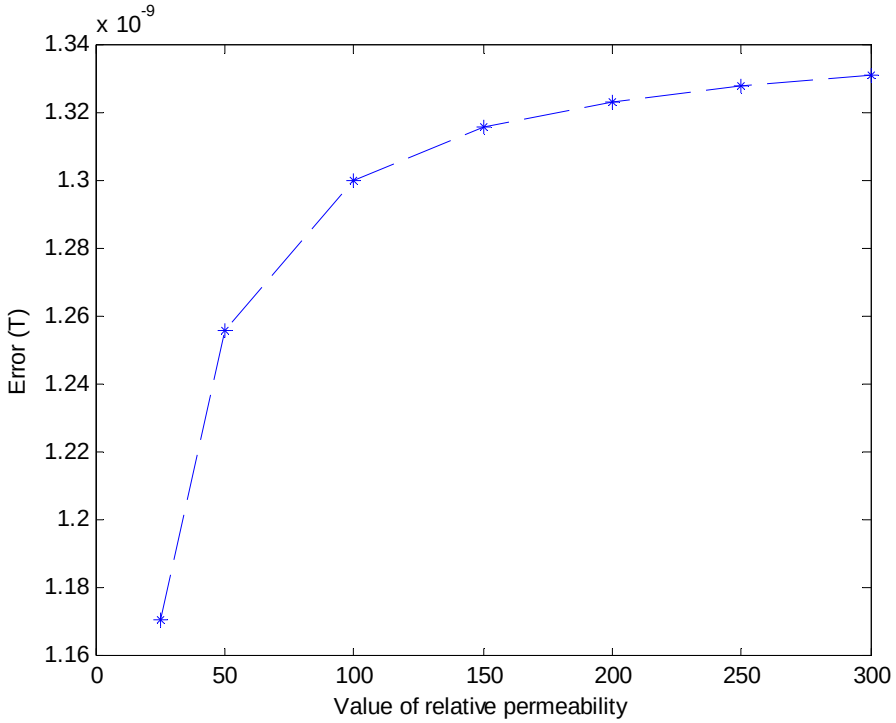

Figure 2.20. B error between stranded core with μ_r =300 and uniform core

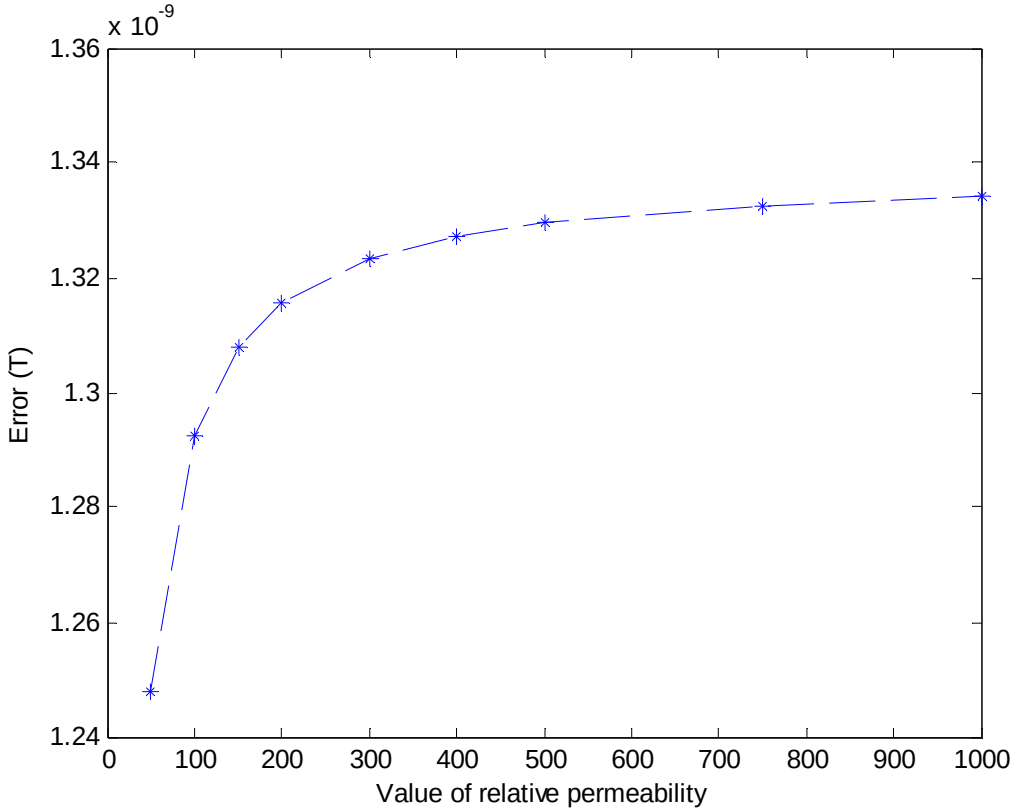

Figure 2.21. B error between stranded core with μ_r =1000 and uniform core

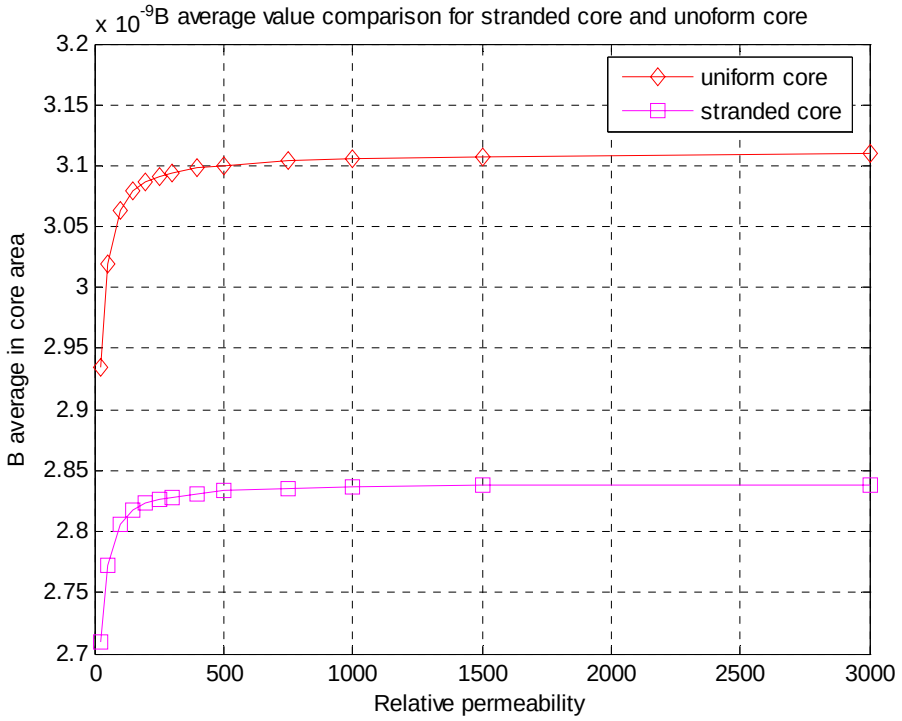

Figure 2.22. Tested B- μ_r data for stranded core and uniform core

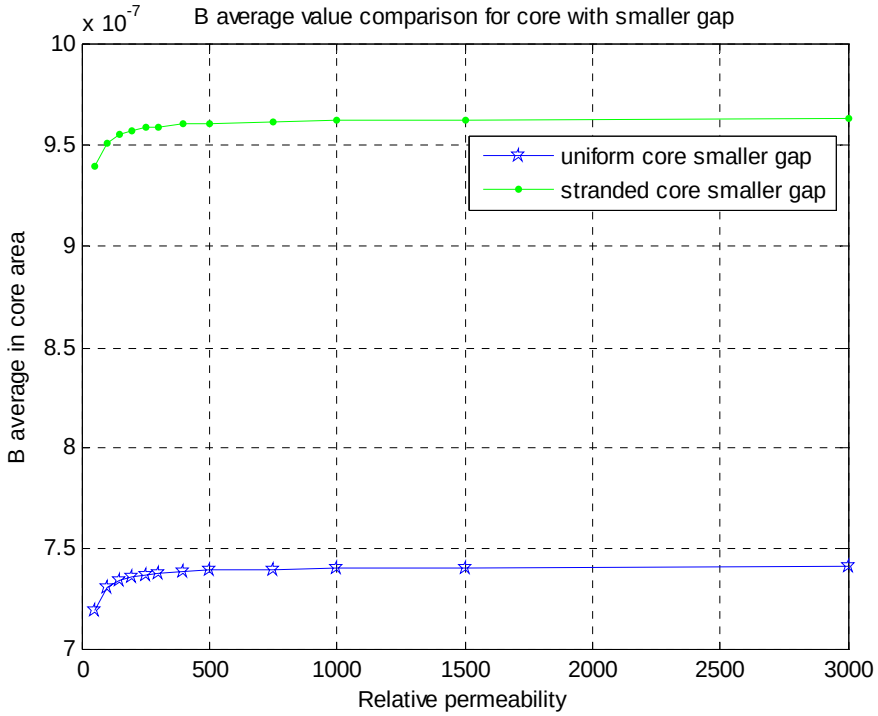

Figure 2.23. Tested B- μ_r data for stranded core and uniform core with a smaller gap

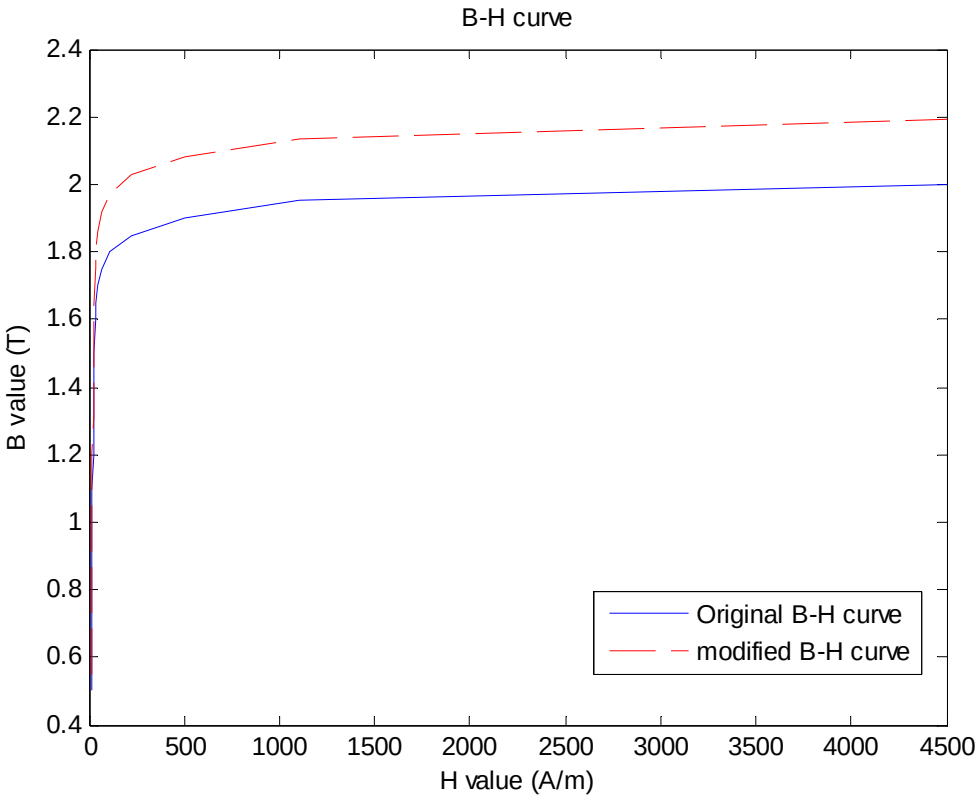

Figure 2.24. Original B-H Curve for stranded core transformer and Modified B-H Curve for uniform core transformer

$B(T)$	$H(A/m)$	$\mu_r = \frac{\mu}{\mu_0} = \frac{B}{\mu_0 H}$
0.5000	11.5	34599
0.6000	13.1	36448
0.7000	14.7	37894
0.8000	16	39789
0.9000	17.1	41883
1.0000	18.3	43485
1.1000	19.6	44661
1.2000	21	45473
1.3000	22	47023
1.4000	24.1	46228
1.5000	27.9	42784
1.6000	33	38583
1.6500	39	33667
1.7000	49	27609
1.7500	65	21425
1.8000	110	13022
1.8500	220	6692
1.9000	500	3024
1.9500	1100	1411
2.0000	4500	354

Table 2.1. Original B-H data for stranded core

Relative permeability of uniform core	25	50	100	150	200
B error ($\times 10^{-9}$)	1.1823	1.2672	1.3118	1.3271	1.3348

Table 2.2. B error between stranded core with μ_r =150 and uniform core

Relative permeability of uniform core	25	50	100	150	200	250	300
B error ($\times 10^{-9}$)	1.1710	1.2559	1.3005	1.3158	1.3235	1.3281	1.3312

Table 2.3. B error between stranded core with μ_r =300 and uniform core

μ_r	50	100	150	200	300	400	500	750	1000
B error ($\times 10^{-9}$)	1.2479	1.2926	1.3078	1.3155	1.3232	1.3271	1.3295	1.3326	1.3341

Table 2.4. B error between stranded core with μ_r =1000 and uniform core

$B_{avg}(T) \times 10^{-9}$	μ_r
2.7098	25
2.7731	50
2.806	100
2.8172	150
2.8229	200
2.8262	250
2.8285	300
2.8313	400
2.8331	500
2.8353	750
2.8365	1000
2.8376	1500
2.8388	3000

Table 2.5. Tested B- μ_r data for stranded core

$B_{avg}(T) \times 10^{-9}$	μ_r
2.9341	25
3.019	50
3.0636	100
3.0789	150
3.0866	200
3.0912	250
3.0943	300
3.0982	400
3.1005	500
3.1036	750
3.1052	1000
3.1069	1500
3.1094	3000

Table 2.6. Tested B-μ_r data for uniform core

Chapter 3. Ansoft Maxwell 3D Modeling

In this chapter, we will calculate the iron loss of a three winding transformer in a 3D model. The manufacturer provides measured data which include the dimensions of transformer, density of core materials, iron loss per pound in different magnetic flux density at frequency of 60 Hz, and B-H curve for core material. In the simulation of Ansoft Maxwell 3D, it is hard to model the stranded core and the software will consume lots of time to compute fields in complex geometry. Therefore, a uniform distributed core is a good choice of substitute for stranded core. We have modified B-H curve which is the main property for a core material.

The original geometry is very complex which will be described in section 3.2. For computational convenience, the model can be simplified as an equivalent model under those two conditions: the equal of core volume and the equal of mean length per turn. The next step is to simulate the simplified model in Maxwell 3D and output data of B field. Although the software can generate 3D mesh automatically, the mesh data can not be obtained. In that way, we need to discretize the core space and compute the center of every mesh element by program. Maxwell 3D can output field value on fixed points. Then, the given B-power loss per pound data is obtained by interpolation. According to B value at every mesh center, a corresponding power loss per pound value can be found. By assembling the volume and power loss per pound at every point, the iron loss of transformer can be achieved.

3.1 Introduction to Ansoft Maxwell 3D

Maxwell 3D is a software for the simulation of electromagnetic fields which can be used to predict the performance of electromagnetic and electromechanical component designs in a virtual environment. It includes 4 solver modules: Transient, AC Magnetic, DC Magnetic and electric field. They are designed to solve problems in both time and frequency domains. Each model uses 3D Finite Elements and automatic adaptive meshing techniques to compute the electrical/electromagnetic behavior of low-frequency components. Maxwell 3D can solve for electromagnetic-field parameters such as force, torque, capacitance, inductance, resistance and impedance as well as generate state-space model, visualize 3D electromagnetic fields, and optimize design performance [19].

In this chapter, we need to use this software to solve field for the 3D simplified transformer model and output the magnetic flux density at selected points in core material.

3.2 Simplified three winding transformer model

The geometry and dimensions of original transformer model is shown in Figure 3.1. The inner winding and outer winding are both low voltage windings. The middle winding is high voltage winding. Outside the three concentric windings are eight identical pieces of core.

Our goal is to output the magnitude of B in the center of every mesh element and the corresponding volume of the mesh element. The geometry of original eight-piece transformer is hard to operate and will involves many additional works. Therefore, an equivalent simplified transformer model is constructed and analyzed first.

The conditions of equivalent for two transformers are stated as: the equal of core volume and the equal of mean length per turn. Based on these two conditions, we can build a simplified transformer model shown in Figure 3.2.

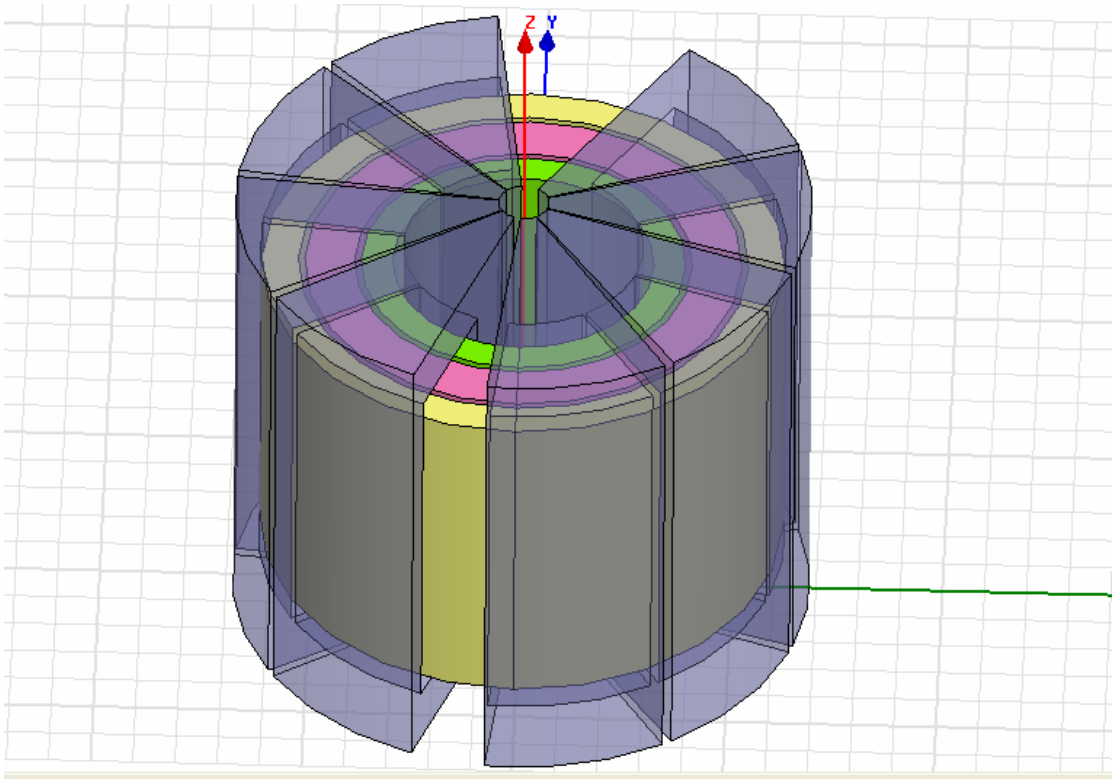

(a). Geometry of original eight-piece core transformer

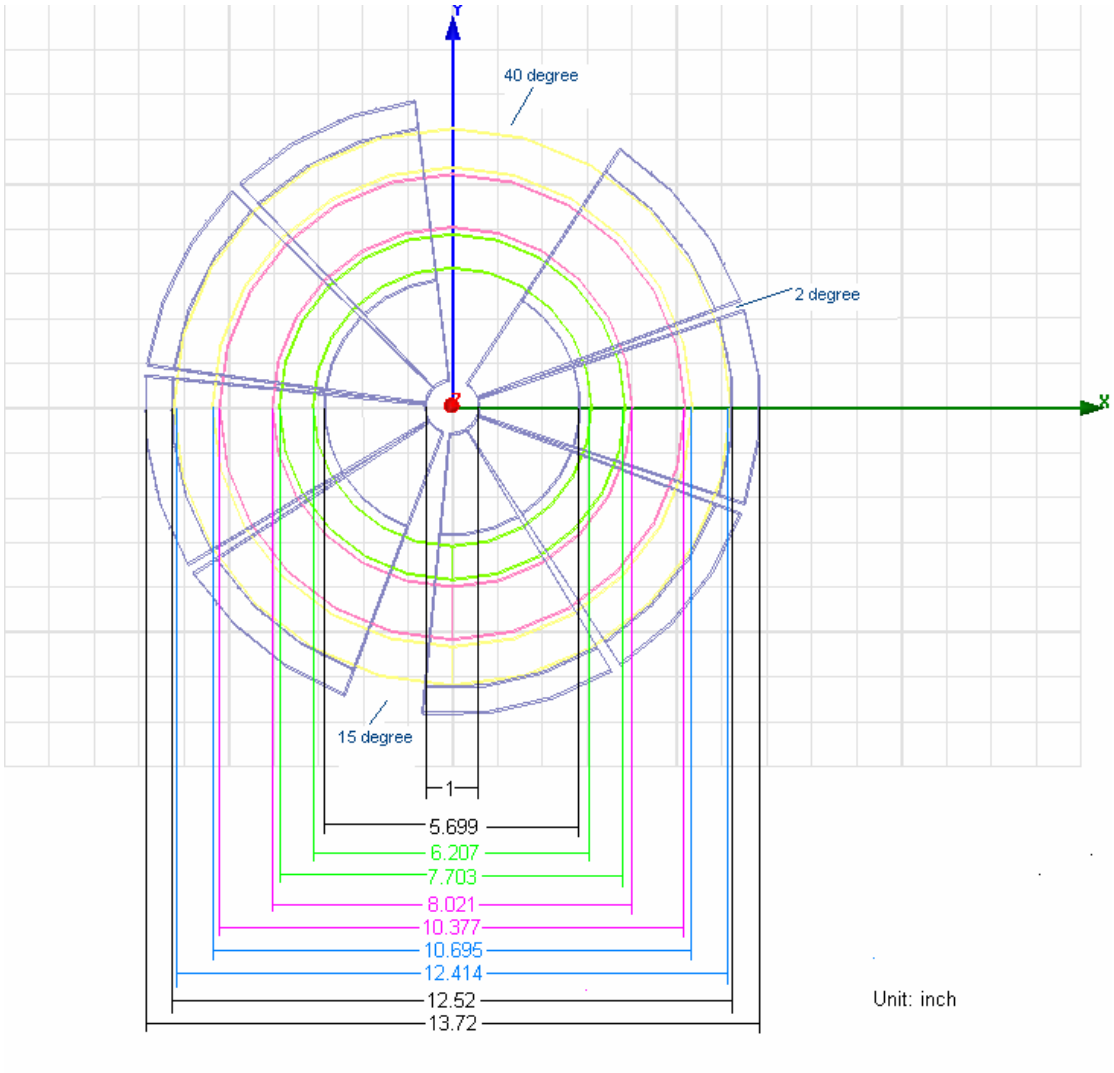

(b). Dimensions of eight-piece core transformer (top view)

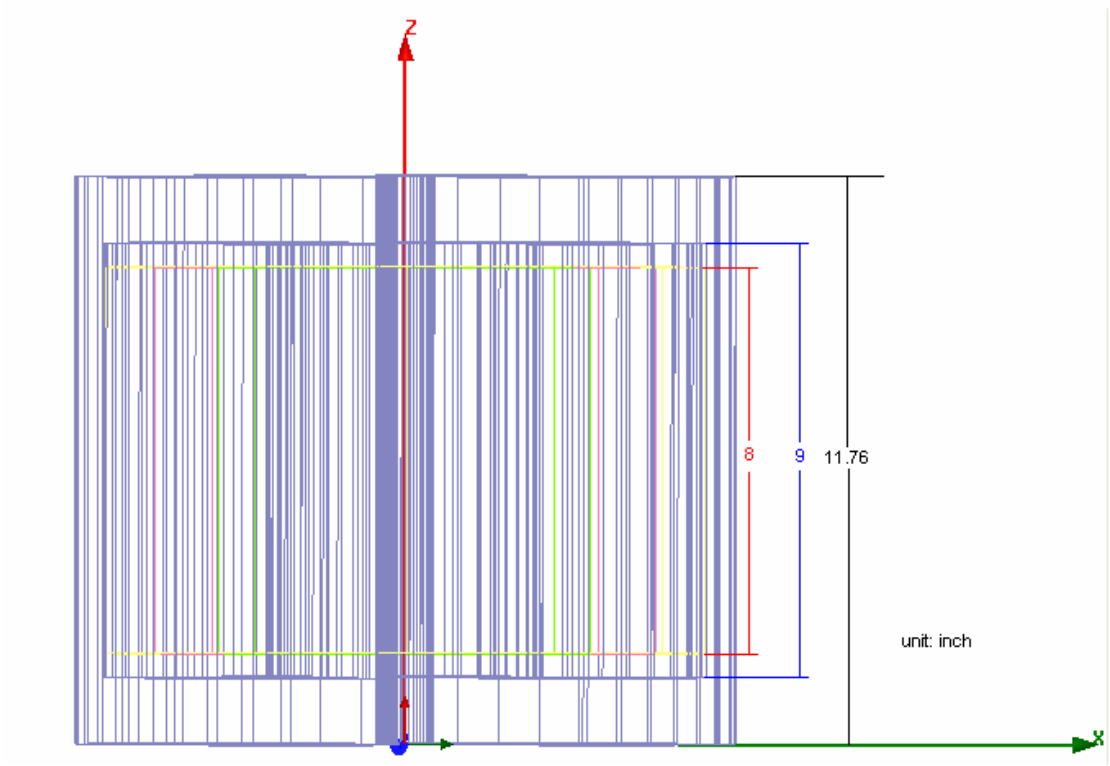

(c). Dimensions of eight-piece core transformer (side view)

Figure 3.1. Geometry and dimensions of eight-piece core transformer

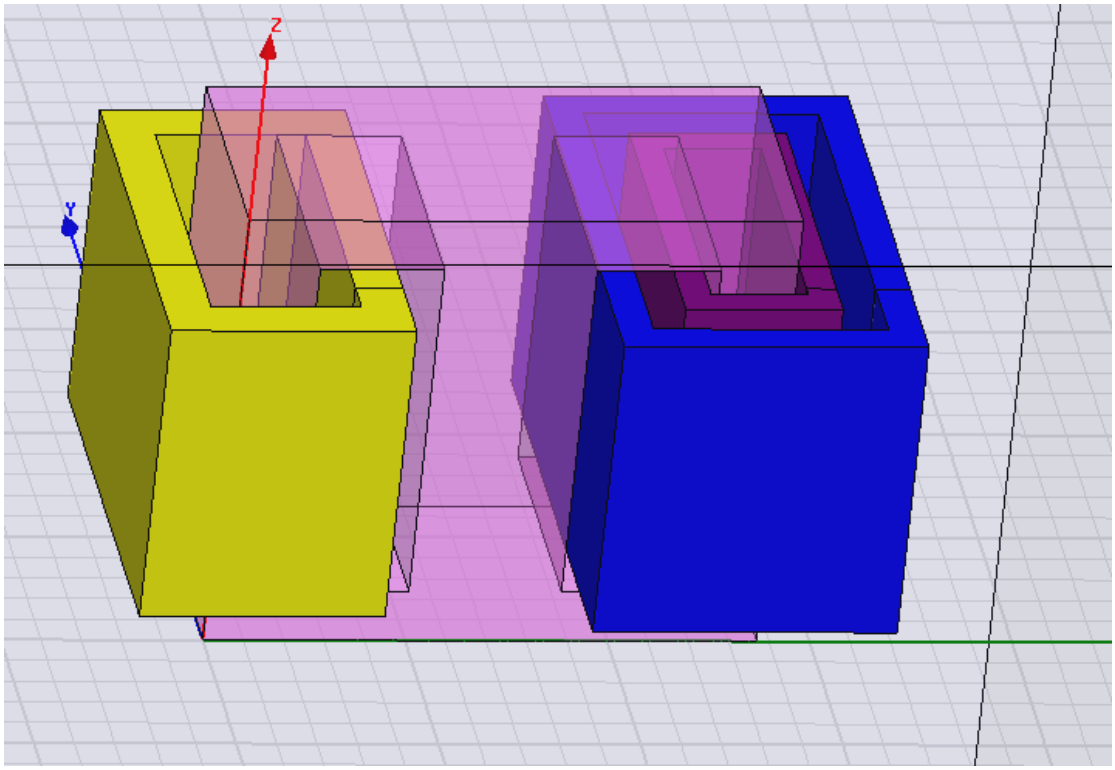

Figure 3.2. Simplified transformer model

3.3 General formulation of transformer loss

The total loss of transformer is mainly made of two components: copper loss (winding) and core loss. The core loss is determined by the volume integration of the core loss per unit volume,

$$P_{core} = \int_V p_{v,T}(B)dV = \sum_{i=1}^{N} p_{v,T}(B_i)\Delta V_i \tag{3.1}$$

where N is the total number of mesh elements of the core, B_i is the flux density at the center of the *i*-th element, ΔV_i is the volume of the *i*-th element.

For a uniform flux density distribution (the same value over the entire core region), the total core loss is the loss per unit volume multiply the volume of the core. If the core's mass density is ρ, the estimated loss per pound (for core) will be

$$P_{lb} = \left[\frac{\omega}{\pi}\left(2H_c + K_{hyst}B_p\right)B_p + \frac{\omega^2}{2}K_{eddy}B_p^2\right]\frac{1}{\rho} \tag{3.2}$$

The coefficient K_{eddy} may be determined quite accurately for laminate iron sheet and strands. Let σ_{Fe} be the conductivity of the iron, then

For laminate iron sheet with sheet thickness a,

$$K_{eddy} = (\sigma_{\mathrm{Fe}}a^2)/12 \tag{3.3}$$

For strands of circular cross section of diameter d,

$$K_{eddy} = (\sigma_{\mathrm{Fe}}d^2)/32 \tag{3.4}$$

From Equation (3.3) and Equation (3.4), we can see the coefficient K_{eddy} is reduced which makes a notable reduction in the iron loss when stranded core material is used.

3.4 Maxwell 3D simulation and core loss calculation

In Maxwell 3D project interface, we draw the simplified model in the region and input data of B-H curve obtained from Chapter 2.3.2 for the material of core. The external circuit is shown in Figure 3.3. Mesh generated by Maxwell 3D is shown in Figure.3.4. The magnitude of B field distribution calculated by Maxwell 3D is posted in Figure 3.5.

Figure 3.6 shows the mesh generated by program and the magnitude of B at every mesh center in the core outputted by Maxwell 3D. Table 3.1 lists the data of core loss per pound for the transformer model when B value changed. Then, the data of core loss per pound at every point in Figure 3.6 can be calculated by interpolation. Figure 3.7 is the plot of power loss per pound function. The density of core material is 7.65kg/dm^3. The volume of core is $0.0113\,\text{m}^3$.

Steps to calculate core loss are as follows:

1. Divide the core space into more than 2000 small elements and calculate the coordinate for the center of every element.
2. Use Maxwell 3D to model the 3D simplified transformer model and analyze B field in core pace.
3. Input points calculated in step 1 to Maxwell 3D and output the B field magnitude in selected points.
4. According to the B field magnitude in selected points, find the corresponding power loss per pound values at center points of elements from Figure 3.7.
5. Plug all the data into Equation (3.1) and we can obtain the final result of iron loss.

$$P_{core} = 81.3W \tag{3.5}$$

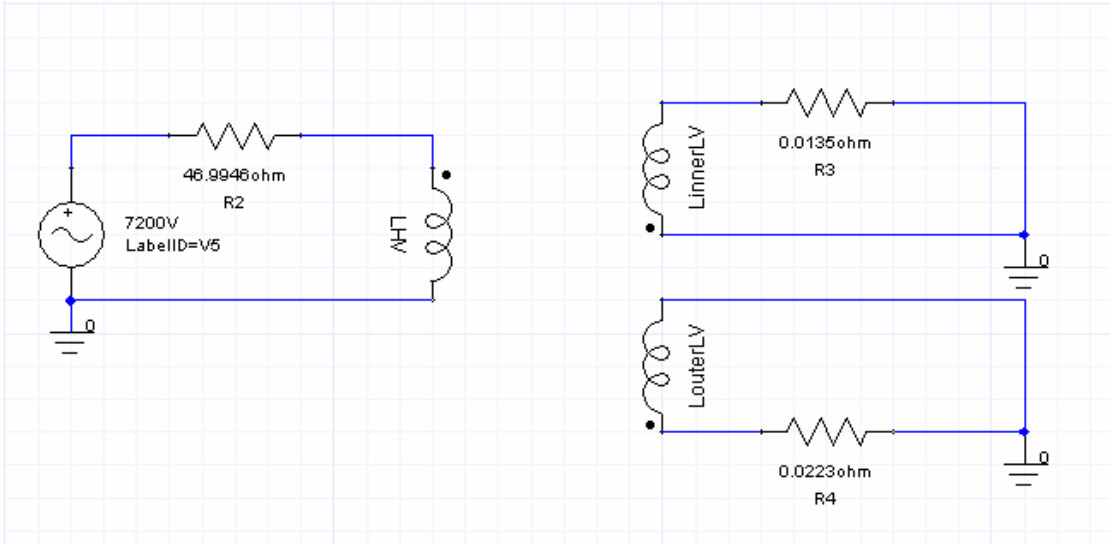

Figure 3.3. External circuit of transformer

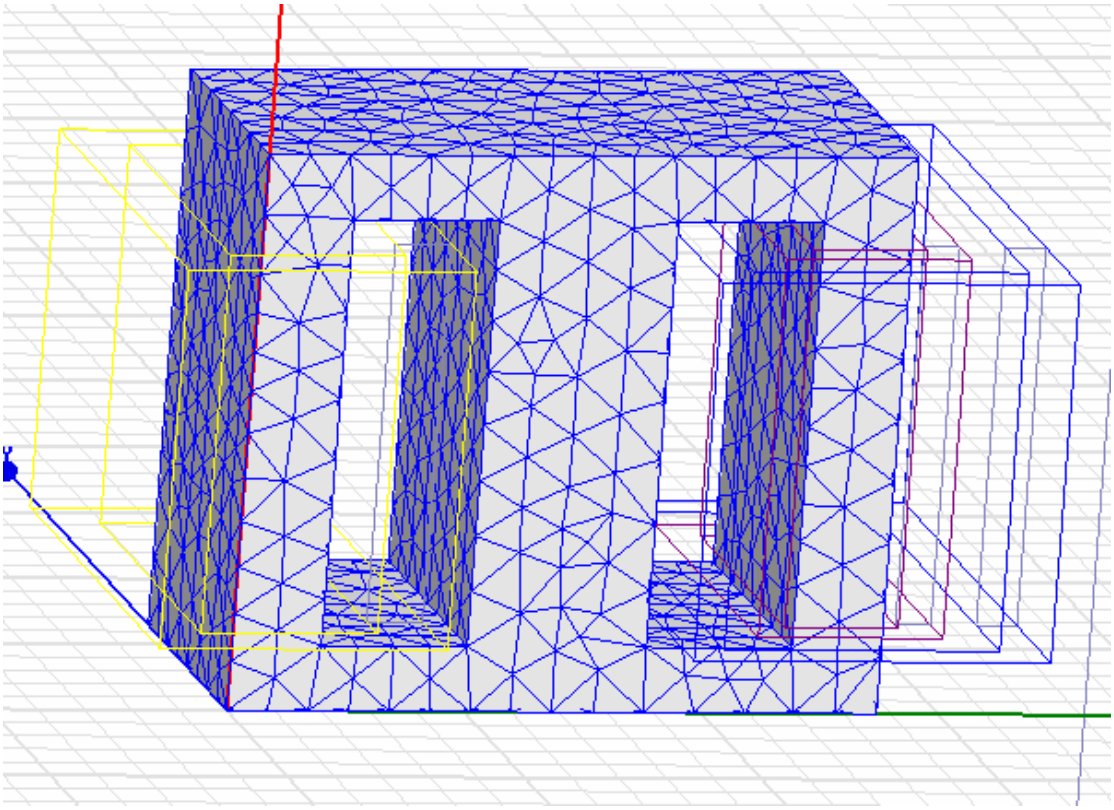

Figure 3.4. Mesh generated by Maxwell 3D

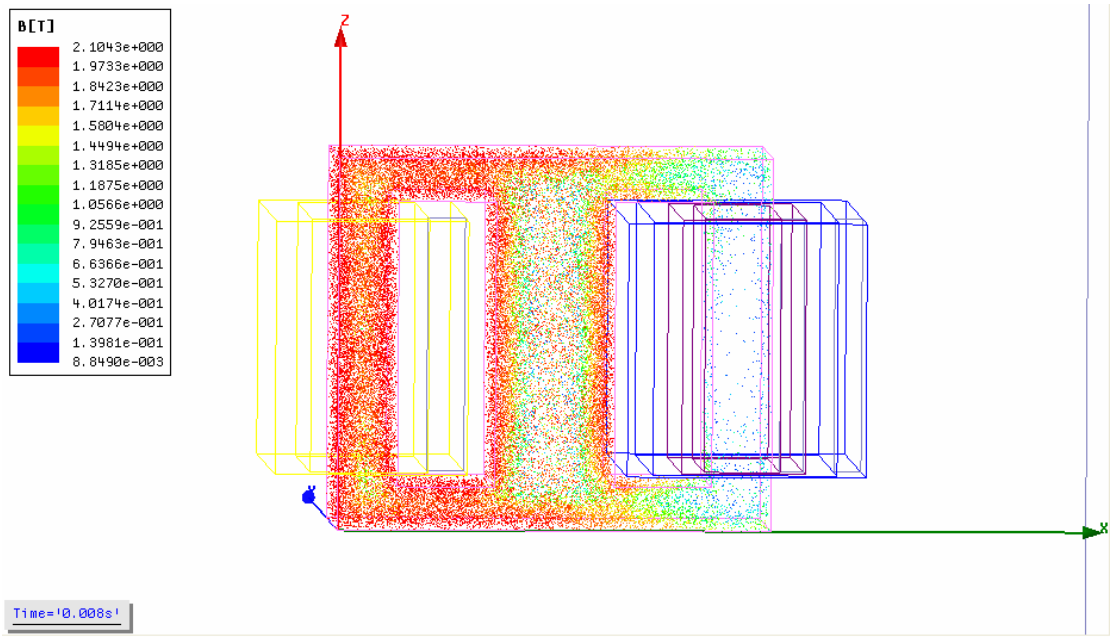

Figure 3.5. B magnitude distribution via Maxwell 3D

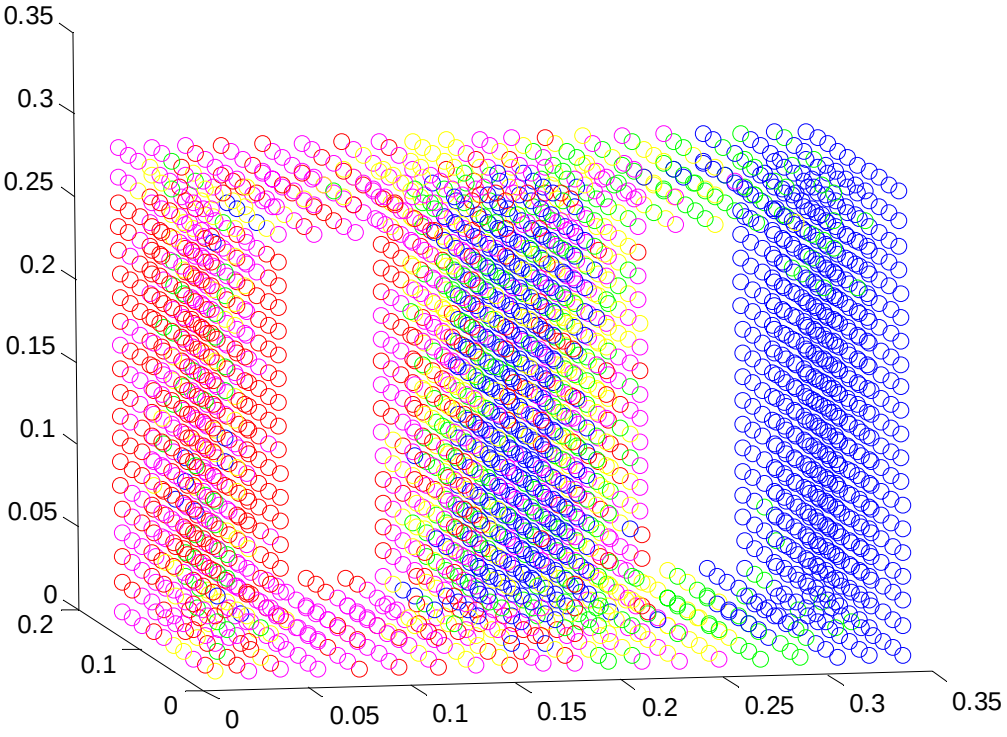

Figure 3.6. Outputted B magnitude data at fixed points

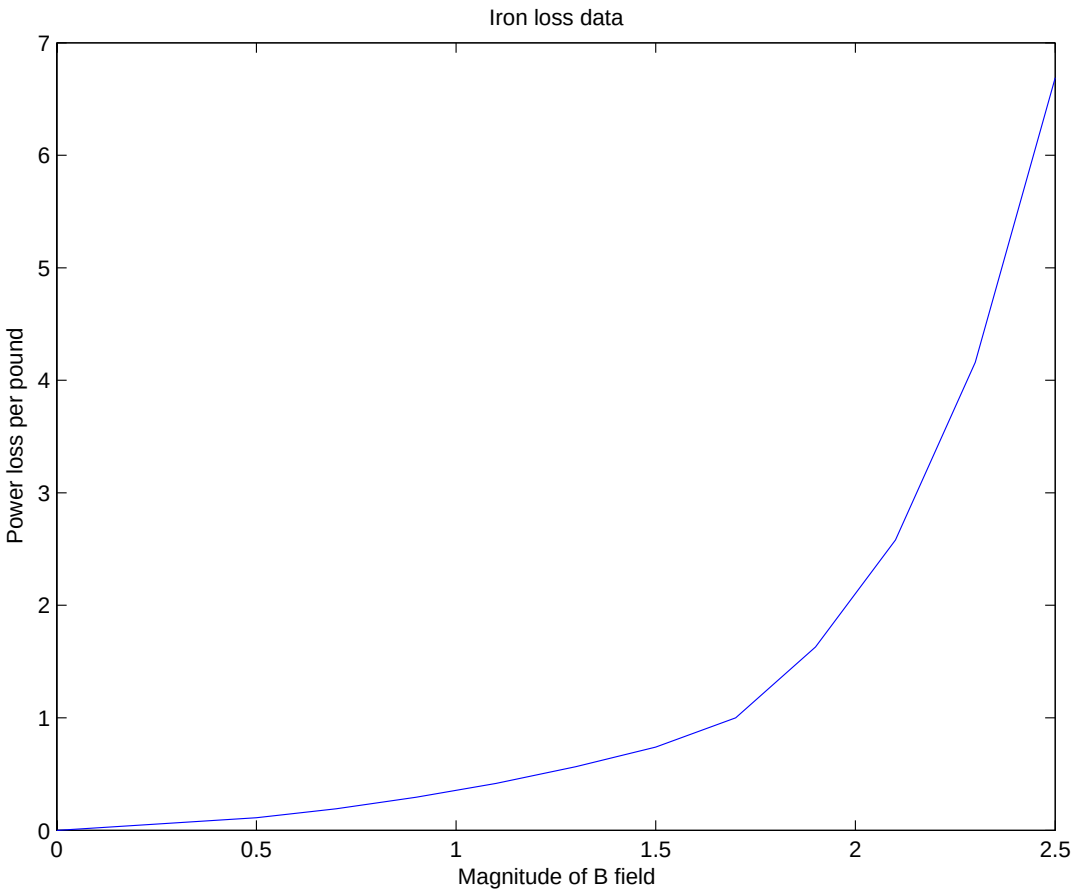

Figure 3.7. Power loss data

B (T)	0	0.5	0.7	0.9	1.1	1.3	1.5	1.7	1.9	2.1
Loss (W/Kg)	0	0.112	0.192	0.294	0.416	0.565	0.740	1.00	1.63	2.58

Table 3.1. Core loss per pound provided by manufacturer

Chapter 4. Conclusion

In this thesis, A 2D finite element method for magnetostatic field and Ansoft Maxwell 3D are adopted to predict the core loss of a three winding transformer. Model simplification and data approximation are important approaches in engineering. The stranded core which has a complex geometric dimension is simplified as a uniform distributed core. In order to keep the accuracy of power loss prediction, the B-H curve of the stranded core which the manufacturer provides needs to be corrected for uniform core. The calculation of modified B-H curve is implemented by finite element method which has been validated by three magnetostatic cases. The original 3D model of the three winding transformer has an inconvenient geometry which has eight pieces of core. Therefore, an equivalent model under the rules of equal core volume and equal mean length per turn is produced in a rectangular shape for easy discretization of mesh. Maxwell 3D is used to create the equivalent model and solve for the field. The output B field data on every mesh center and the corresponding power loss per pound need to be assembled with the density of core material and volume of every mesh element to acquire the prediction of core loss in three-winding stranded core transformer.

The whole procedure still needs improvement. For the 2D nodal basis finite element method, the matrix solving is very time consuming. An improved algorithm is necessary to enhance the efficiency. The accuracy of this prediction can be improved by adopting numerical method to calculate the modified B-H curve for uniform core.

References

[1] M. Okabe, M. Okada and H. Tsuchiya, “Effects of Magnetic Characteristics of Materials on the Iron Loss in the Three Phase Transformer Core”, *IEEE Trans. Magn*, vol. MAG-19, no.5, pp. 2192-2194, September 1983.

[2] M. Chiampi, A. L. Negro and M. Tartaglia, “A Finite Element Method to Compute Three Dimensional Magnetic Field Distribution in Transformer Cores”, *IEEE Trans. Magn*, vol.MAG-16, no.6, pp. 1413-1419, November 1980.

[3] M. V. K. Chari, A. Konrad, Z. J. Csendes, P. Silvester and M. A. Palmo, “Three-Dimensional Magnetostatic Field Analysis of Electrical Machinery by the Finite-Element Method”, *IEEE Transactions on Power Apparatus and Systems*, vol.PAS-100, no.8, pp. 4007-4013, August 1981.

[4] N. A. Demerdash, T. W. Nehl, O. A. Mohammed and F. A. Fouad, “Experimental Verification and Application of the Three Dimensional Finite Element Magnetic Vector Potential Method in Electrical Apparatus ”, *IEEE Transactions on Power Apparatus and Systems*, vol.PAS-100, no.8, pp. 4112-4122, August 1981.

[5] J. Coulomb, “Finite Element Three Dimensional Magnetic Field Computation”, *IEEE Trans. Magn*, vol.MAG-17, no.6, pp. 3241-3245, November 1981.

[6] N. A. Demerdash, T. W. Nehl, F. A. Fouad and O. A. Mohammed, “Three Dimensional Finite Element Vector Potential Formulation of Magnetic Fields in Electrical Apparatus ”, *IEEE Transactions on Power Apparatus and Systems*, vol.PAS-100, no.8, pp. 4104-4110, August 1981.

[7] S. Bobbio, P. Alotto, F. Delfino, P. Girdinio and P. Molfino, “Equivalent Source Methods for 3-D Force Calculation With Nodal and Mixed FEM in Magnetostatic Problems”, *IEEE Trans. Magn*, vol.37, no.5, pp. 3137-3140, September 2001.

[8] C. Kaehler and G.. Henneberger, “Transient 3-D FEM Computation of Eddy-Current Losses in the Rotor of a Claw-Pole Alternator”, *IEEE Trans. Magn*, vol.40, no.2, pp. 1362-1365, March 2004/

[9] M. Dorica and D. D. Giannacopoulos, “Impact of Mesh Quality Improvement Systems of the Accuracy of Adaptive Finite-Element Electromagneitcs With Tetrahedra”, *IEEE Trans. Magn*, vol.41, no.5, pp. 1692-1695, May 2005.

[10] X. C. Wei, E. P. Li and Y. J. Zhang, “Efficient Solution to the Large Scattering and Radiation Problem Using the Improved Finite-Element Fast Multipole Method”, *IEEE Trans. Magn*, vol.41, no.5, pp. 1684-1687, May 2005.

[11] J. Jin, *The finite element method in electromagnetics* (2nd edition). New York: Wiley, 2002.

[12] S. J. Salon and J. M. Schneider, “Formulation of Poisson’s Equation”, *IEEE Trans. Magn*, vol.MAG-16, no.6, pp. 1413-1419, November 1981.

[13] O. C. Zienkiewicz, *The finite element method* (fourth edition). McGraw-Hill Book Company(UK), 1989.

[14] W. H. Hayt, Jr and John A. Buck, *Engineering Electromagnetics* (6th edition). New York: McGraw-Hill, 2001.

[15] Caicheng Lu, Mesh27 user manual (internal reference), University of Kentucky, 2007.

[16] M. Kihara, “An introduction to Electromagnet Design”, June 2000.

[17] J. Karn and R. Wines, “Finite Element Modeling of Permeability Differences in CEBAF Dipoles”, J-Lab, TN, 1999.

[18] G. Liu, X. Xu, “Improved Modeling of the Nonlinear B-H Curve and Its Application in Power Cable Analysis”, *IEEE Trans. Magn*, vol.38, no.4, pp. 1759-1763, July 2002.

[19] Ansoft, Maxwell 3D, product overview, Maxwell 3D user manual, 2006.

Vita

The author of this thesis was born in the city of Xi' an, P. R. China, June 12th, 1984. She finished her undergraduate study in Xidian University at Xi' an, China and got her Bachelor's degree in July 2006. During her undergraduate study, she worked in the Digital Signal Processing Lab in Xidian University instructed by Professor Wanyou Guo (Dec. 2005-Jun. 2006, Xi' an, China). She was honored with the University Scholarships for 3 consecutive years in Xidian University (2003-2005).